Article

Comparing Pixel- and Object-Based Approaches for Classifying Multispectral Drone Imagery of a Salt Marsh Restoration and Reference Site

Gregory S. Norris [1], Armand LaRocque [1,*], Brigitte Leblon [2], Myriam A. Barbeau [3] and Alan R. Hanson [4]

[1] Faculty of Forestry and Environmental Management, University of New Brunswick, Fredericton, NB E3B 5A3, Canada; gnorris1@unb.ca
[2] Faculty of Natural Resource Management, Lakehead University, Thunder Bay, ON P7B 5E1, Canada; bleblon@lakeheadu.ca
[3] Department of Biology, University of New Brunswick, Fredericton, NB E3B 5A3, Canada; mbarbeau@unb.ca
[4] Canadian Wildlife Service, Environment Canada, P.O. Box 6227, Sackville, NB E4L 4N1, Canada; al.hanson@ec.gc.ca
* Correspondence: larocque@unb.ca

Abstract: Monitoring salt marshes with remote sensing is necessary to evaluate their state and restoration. Determining appropriate techniques for this can be overwhelming. Our study provides insight into whether a pixel- or object-based Random Forest classification approach is best for mapping vegetation in north temperate salt marshes. We used input variables from drone images (raw reflectances, vegetation indices, and textural features) acquired in June, July, and August 2021 of a salt marsh restoration and reference site in Aulac, New Brunswick, Canada. We also investigated the importance of input variables and whether using landcover classes representing areas of change was a practical way to evaluate variation in the monthly images. Our results indicated that (1) the classifiers achieved overall validation accuracies of 91.1–95.2%; (2) pixel-based classifiers outperformed object-based classifiers by 1.3–2.0%; (3) input variables extracted from the August images were more important than those extracted from the June and July images; (4) certain raw reflectances, vegetation indices, and textural features were among the most important variables; and (5) classes that changed temporally were mapped with user's and producer's validation accuracies of 86.7–100.0%. Knowledge gained during this study will inform assessments of salt marsh restoration trajectories spanning multiple years.

Keywords: image classification; ecological restoration; wetland; pixel-based image analysis; object-based image analysis; Random Forest; Bay of Fundy

1. Introduction

Although wetlands occupy approximately 2–6% of the earth's surface, they fulfill many ecological functions [1,2]. Wetlands provide carbon sequestration [3,4]; support soil formation and stabilization [5,6]; supply food, water, and plant biomass [7–9]; and serve as cultural and recreational areas [10,11]. The quality and quantity of ecosystem services provided by wetlands varies depending on their type, hydrology, water chemistry, soils, and plant species [12–15]. Unfortunately, global wetland loss has been extensive because of anthropogenic activities, including agriculture, urbanization, aquaculture, and industry, as well as climate change [16,17]. Major efforts are being made to restore wetlands and the beneficial services they provide [18–21]. Understanding vegetation dynamics during wetland restoration can aid in assessing and modeling the recovery trajectory, evaluating ecosystem services, and planning future restoration projects [22,23].

The ecological importance of wetlands and their vegetation dynamics highlight the need for reliable, accurate, and efficient methods to monitor vegetation changes. Remote sensing offers practical ways to monitor vegetation distributions in areas that are difficult to

access on foot, including wetlands. Indeed, many initiatives to create wetland classification systems and inventories (maps displaying the extent and distribution of wetlands over a geographical area) have been made at regional, national, and international scales [24,25]. The wetlands of interest in our study were coastal salt marshes in Atlantic Canada, which have been part of the Canadian Wetland Classification System since its development in 2002 [24,25].

Aerial imagery acquired using sensors fixed to planes [26–28] and satellites, including Sentinel [29], Landsat [30–33], Worldview [33], and others [34], has been successfully used for mapping coastal wetlands. Very-high-spatial-resolution aerial imagery can be acquired using sensors fixed to drones, which have recently (compared to planes and satellites) become popular tools for environmental monitoring and have also been used to map coastal wetland vegetation and its changes [35–41]. Prior to the development of very-high-spatial-resolution drone and satellite imagery, which are especially valuable for assessing differences in heterogeneous wetland communities with species composition differing at the scale of centimeters [42], a prevalent challenge in mapping wetlands (including salt marshes) was that the spatial resolution of images was too low to assess fine-scale ecological dynamics [43]. Lower-resolution satellites (e.g., Landsat) have typically been restricted to assessing regional extent and loss of marshes [30–33]. Despite the desire for higher-spatial-resolution imagery for mapping coastal wetlands, such resolution does not always equate to higher classification accuracy [44], especially as classifications become more complicated with additional landcover classes that can now be detected. In addition to achieving very high resolution, using drone imagery for environmental monitoring is cost- and user-friendly compared to imagery acquired with conventional air- and spacecraft. Drones operate beneath cloud cover and can be deployed whenever the weather permits, making image acquisition at regular temporal intervals possible and facilitating analysis of vegetation dynamics [45]. As additional images are added to a set of multi-temporal images, however, the time associated with fieldwork, image acquisition, and image processing increases the complexity and financial cost of a monitoring project. Overall, there are many considerations when planning an environmental monitoring project using remote sensing techniques, including which image classification methods are most appropriate.

Much effort has been made to develop image classification methods for vegetation mapping and change analysis, including traditional pixel-based (PB) [46,47] and, more recently, object-based (OB) methods [47,48]. Differences in these methods are attributed to the fundamental unit of analysis. For PB techniques, this is an image pixel, while for OB techniques, image objects (groups of pixels) are first created using image segmentation. Selecting the appropriate method depends partially on the sizes of the features of interest and the spatial resolution of the imagery. PB classification approaches have typically been used for wetland mapping in Canada [25], but OB classification is preferred when objects of interest are substantially larger than the spatial resolution of pixels, which is common when using very-high-spatial-resolution drone imagery [48]. Image segmentation can, however, introduce over- and under-segmentation errors by incorrectly grouping pixels where segments do not represent the heterogeneity of plant communities [49,50]. Selecting optimal segmentation settings for an entire wetland landscape can be challenging due to the potential ranges of wetland vegetation sizes [51]. Among studies specifically investigating whether PB or OB methods are more suitable for classifying imagery acquired over coastal wetlands [50,52], Martinez Prentice et al. [50] found that PB classification slightly out-performed OB classification for wetlands in Estonia, while Zheng et al. [52] found that OB outperformed PB for wetlands in China. When inspecting studies in other wetland environments that use very-high-spatial-resolution multispectral images but do not directly compare classification approaches, there is a preference for using OB methods [27,40,44,53] over PB methods [37]. Within a PB or OB framework (i.e., using either pixels or objects as the base unit of image analysis), many commonly used classification algorithms can be applied for mapping coastal wetland vegetation, such as machine learning algorithms, including Maximum Likelihood [32], Support Vector Machine [40], and

Random Forest (RF) [33,34,36,40,50,54]; deep learning algorithms, including Artificial Neural Networks [38,44,52]; K-Nearest Neighbours [27]; etc. In general, many studies have investigated the suitability of the available classification algorithms for coastal wetlands and obtained varying results. Among machine learning algorithms, Random Forest is often one of the highest performing [25,52]. A lack of consensus indicates that more research is needed to determine which classification approach, including the base unit of analysis (pixel- or object-based) and algorithm (RF, etc.), is best for mapping vegetative communities of coastal wetlands, including the salt marshes of Atlantic Canada.

Our study navigates the intricate task of selecting effective techniques for monitoring salt marshes through remote sensing, aiming to streamline the process of choosing classification methods tailored for salt marsh mapping in Atlantic Canada. Using drone imagery captured during the growing season of June, July, and August 2021 at a salt marsh restoration and reference site in Aulac, New Brunswick, we sought to identify the optimal Random Forest classification approach—considering both pixel- and object-based methods—for mapping the vegetation within these marshes. Our landcover classes included single and mixed plant species, bare ground, water, various substratum types typical of salt marshes, as well as specific classes to assess monthly image variations (change classes) [46,55,56]. We delved into key input variables for classification, such as reflectance information, vegetation indices, and textural features, and so incorporated a more extensive array of input image variables compared to other remote sensing studies in salt marsh mapping. By evaluating the importance of input variables from June, July, and August, our study provided insight into the value of multi-temporal classification and the times of year that contribute most to achieving high classification accuracy. Our ultimate goal is to guide future classification and change-detection projects in the relatively understudied salt marshes of Atlantic Canada (and other north temperate geographic locations), providing valuable insights for selecting classifiers when using multispectral drone imagery to monitor them.

2. Materials and Methods

2.1. Study Area

The study area in Aulac is located at the head of the Cumberland Basin within the Bay of Fundy (latitude: 45°51′31″N, longitude: 64°18′15″W; Figure 1). Semi-diurnal tidal amplitudes in the Cumberland Basin reach more than 12 m [57]. A managed realignment salt marsh restoration project began here in 2009 under the leadership of Ducks Unlimited Canada (DUC) and partners [23,58–60]. The project consists of two restoration (B, C) and two reference (A, D) sites; the study areas of focus for the present paper were the Western reference and restoration sites (A and B, Figure 1). Among the plant taxa present in the sites, we were particularly interested in mapping ecologically significant ones, namely, *Spartina alterniflora* (saltwater cordgrass, syn. *Sporobolus alterniflorus*; [61,62]) and *Spartina patens* (salt marsh hay, syn. *Sporobolus pumilus*), which are central during restoration [23,60]. We used imagery from when the restoration was in its 11th year (2021) after dike breach, and the low-elevation bioengineer species of salt marshes in eastern North America, *S. alterniflora*, dominated the site. The reference site is mainly mid-elevation salt marsh dominated by *S. patens* (typical of Bay of Fundy salt marshes [60]), with *S. alterniflora* restricted to creeks and seaward edges. Other vegetation present in the sites were terrestrial species growing on the high-elevation dike, and coastal species freshwater cordgrass (*Spartina pectinata* (syn. *Sporobolus michauxianus*)) and seaside arrowgrass (*Triglochin maritima*). Species growing in low densities and usually mixed with other vegetation included maritime orach (*Atriplex* spp.), sea lavender (*Limonium carolinianum*), seaside alkali grass (*Puccinellia maritima*), seablite (*Suaeda* spp.), sea milkwort (*Lysimachia maritima*), seaside plantain (*Plantago maritima*), seaside goldenrod (*Solidago sempervirens*), and sea glasswort (*Salicornia maritima*) [59]; hereafter, we refer to these various plants by their genus names, except for the *Spartina* grasses. The phenological growing period of vegetation in these marshes is from early June, when above-ground biomass first emerges from below-ground roots and rhizomes, to late September, when plants begin to senesce [23].
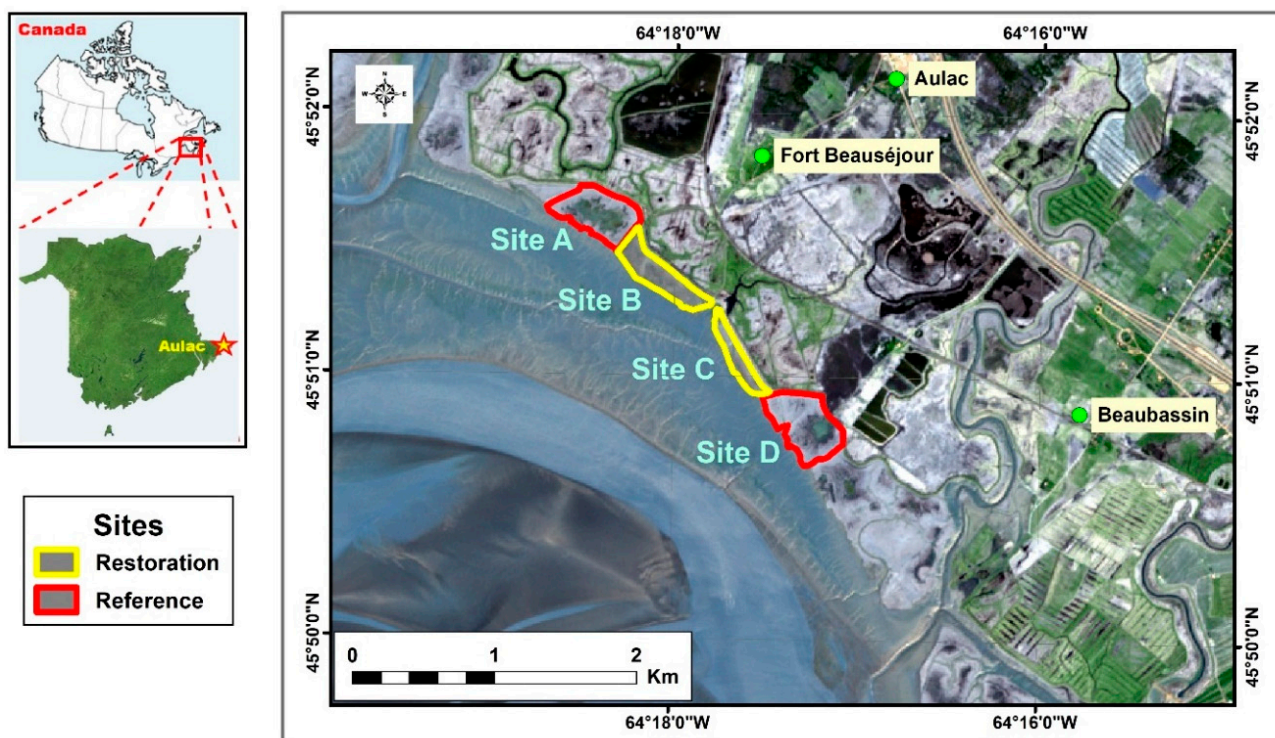
Figure 1. Location of studied salt marshes in Aulac, New Brunswick, in a Google Earth™ image of New Brunswick (insert); details include restoration sites (outlined in yellow) and reference sites (red). The sites examined in our paper were A and B.

2.2. Field Data

Field data were collected on 11 June, 11 July, and 8–10 August 2021, using stratified random sampling with quadrats (0.5 × 0.5 m) along three transects in the reference site and four transects in the restoration site (15 quadrats transect^{-1} sampling round^{-1}). In addition, the perimeter of the sites was surveyed on foot to ensure that all landcover classes were documented. Within each quadrat, the landcover class was recorded, and plant stems were identified and counted. Photographs and GPS points were acquired for each quadrat location. Between the two sites, a total of 30 classes were identified using field data and mosaics of each month's imagery displayed in true and false colour (Table 1).

Table 1. Names and descriptions of landcover classes used in the study. Corresponding class number and colour codes included. Classes 1–15 were used in the classification of the restoration site (Site B), and classes 1–9 and 16–30 were used in the classification of the reference site (Site A). See Supplementary Table S1 for photographs of the vegetation classes and Supplementary Figures S1 and S2 for photographs of the other classes.

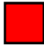| Class Number	Class Color Code	Name	Description
1		Bare mud exposed to air	Bay of Fundy mud beyond the seaward edges of the sites.
2		Compacted soil (dark)	Compacted soil along the seaward edges of the sites as a result of past dike construction.
3		Rocks/eroded shoreline pieces	Rocks washed up on shore. Also includes large chunks of shoreline that eroded from the edge of the sites.

Table 1. *Cont.*
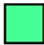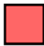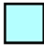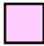
Class Number	Class Color Code	Name	Description
4		Wrack	Dead grass and algae that accumulated into mats and washed onto the sites.
5		*Spartina alterniflora* (muddy)	Assemblage dominated by saltwater cordgrass (*Spartina alterniflora*), the low-elevation bioengineer species of salt marshes in the region, with blades covered with some tidal mud.
6		*Spartina alterniflora* (clean, dense)	Assemblage dominated by saltwater cordgrass (*S. alterniflora*) that is not muddy and is growing densely
7		*Spartina patens*	Assemblage dominated by salt marsh hay (*Spartina patens*), the mid-elevation bioengineer species of salt marshes in the region.
8		Deep salt pool water	Deep water contained in salt pools (depressions in the marsh that retain water at low tide).
9		Bare mud exposed to air (June) → clean *S. alterniflora* growing in dense assemblages (July, August)	Bay of Fundy mud in the June imagery which is colonized by *S. alterniflora* in the July and August imagery.
10		Compacted soil (light)	Highly compacted soil that appears light in the imagery, likely due to high sand and/or salt content.
11		Wood	Woody debris that has been washed into the site or remnants of past dike construction.
12		*Spartina pectinata*	Freshwater cordgrass (*Spartina pectinata*) occupying high-elevation areas next to the dike.
13		*S. alterniflora* (clean, sparse)	Saltwater cordgrass (*S. alterniflora*) that is not muddy and is growing in sparse assemblages.
14		*S. alterniflora* → Wrack	Areas of *S. alterniflora* in June and July that became covered in wrack by August.
15		Dike vegetation	Unidentified terrestrial plant species that grow on top of the high-elevation dike areas.
16		*Triglochin maritima*	Assemblage dominated by seaside arrowgrass (*Triglochin maritima*), a common salt marsh plant with fleshy dark-green stems.
17		Mixed mid-elevation vegetation (*S. patens, Puccinellia*, etc.)	Mixed assemblages of vegetation, including *S. patens, Puccinellia maritima, Lysimachia maritima, Plantago maritima, Solidago sempervirens, Argentina anserina*, and *Limonium carolinianum*.
18		Floating green algae	Green algae (Chlorophyta) floating on top of salt pool water.
19		Emerged salt pool mud (June) → shallow salt pool water (July, August)	Mud within salt pools that was exposed to the air in the June imagery and covered in water in the July and August imagery. Water level is variable in salt pools and controlled by evaporation, spring tides, and rain events.
20		Emerged salt pool mud (salty)	Mud within salt pools that was exposed to the air in the imagery of each month.
21		Submerged aquatic vegetation	Underwater *Ruppia maritima* and Chlorophyta in salt pools.

Table 1. *Cont.*

Class Number	Class Color Code	Name	Description
22		Deep salt pool water (June) → floating green algae (July, August)	Deep water contained in salt pools in the June imagery which becomes covered in floating green algae in the July and August imagery.
23		Deep salt pool water (June) → submerged aquatic vegetation (July, August)	Deep water contained in salt pools in the June imagery which becomes submerged aquatic vegetation in the July and August imagery.
24		Deep salt pool water (June, July) → submerged aquatic vegetation (August)	Deep water contained in salt pools in the June and July imagery which becomes submerged aquatic vegetation in the August imagery.
25		Shallow salt pool water	Shallow water contained in salt pools where the unvegetated pool bottom is visible.
26		Shallow salt pool water (June) → submerged aquatic vegetation (July, August)	Shallow water contained in salt pools in the June imagery which becomes submerged aquatic vegetation in the July and August imagery.
27		Floating green algae (June) → submerged aquatic vegetation (July) → shallow salt pool water (August)	Floating green algae (Chlorophyta) in the June imagery which becomes submerged aquatic vegetation in the July imagery and shallow salt pool water in the August imagery.
28		Floating green algae (June) → deep salt pool water (July, August)	Floating green algae (Chlorophyta) in the June imagery which becomes deep salt pool water in the July and August imagery.
29		Wrack (June) → vegetated areas of *S. alterniflora* and *S. patens* (July, August)	Wrack in the June imagery which washes away or becomes colonized by vegetation and appears as *S. alterniflora* and *S. patens* in the July and August imagery.
30		Mixed vegetation: *S. alterniflora* and *S. patens*	Mixed assemblages of *S. alterniflora* and *S. patens*.

2.3. Image Acquisition

A MicaSense Dual Camera System (MicaSense, Seattle, WA, USA) mounted on a DJI Matrice 200 V2 aerial drone (DJI, Nanshan District, Shenzhen, China) was used to acquire multispectral drone images of the sites on 13 June, 12 July, and 10 August 2021 (Table 2). The image acquisitions were planned from shortly after the above-ground biomass had emerged (June) until after the vegetation was fully grown and flowering (August) but before it began to senesce (September) [23].

Table 2. Characteristics of multispectral drone images used in the study acquired in Aulac salt marshes in 2021.

Month	Site	Start Time	Tidal Height (m) *	Cloud Cover	Solar Azimuth (°)	Solar Altitude (°)	Course Angle (°)	No. of Images
June	Reference	12:00	6.7	Cumulus	139	63	230	8550
	Restoration	12:33	7.9		155	66	230	7730
July	Reference	12:38	8.9	Stratus	155	64	230	7380
	Restoration	13:05	9.9		170	66	230	7560
August	Reference	10:43	5.5	Stratus	119	45	218	8180
	Restoration	11:14	6.9		128	50	218	7940

(*) Tidal height obtained from the nearby Pecks Point, New Brunswick, tidal station.

The camera system consisted of two five-band multispectral cameras, with the ten bands covering visible and near-infrared spectra (Table 3). Images that had a spatial resolution close to 7 cm were acquired with 80% front and side overlap between them and along a grid pattern at 100 m altitude over the sites and a horizontal speed of 10 m s^{-1}. The

drone was controlled using DJI Pilot mission planner software v1.7.2 (the android version compatible with the DJI CrystalSky Tablet), a DJI Cendence remote controller, and a DJI CrystalSky tablet (Figure 2). Images of the MicaSense Calibrated Reflectance Spectralon Panel (RP04-1949202-OB; Figure 2E) were acquired immediately before and after each flight.

Table 3. Spectral characteristics of the ten bands acquired by the MicaSense Dual-Camera system.

Band Number	Band Name	Center of Wavelength (μm)	Bandwidth (μm)
1	Coastal Blue 444	444	28
2	Blue 475	475	32
3	Green 531	531	14
4	Green 560	560	27
5	Red 650	650	16
6	Red 668	668	14
7	Red Edge 705	705	10
8	Red Edge 717	717	12
9	Red Edge 740	740	18
10	NIR 842	842	57

Figure 2. Photographs of (**A**) DJI Matrice V2 aerial drone and MicaSense Downwelling Light Sensor (DLS), (**B**) airborne drone showing the MicaSense Dual Camera System, (**C**) DJI Cendence remote controller, (**D**) DJI CrystalSky tablet with DJI Pilot software, and (**E**) Spectralon panel (RP04-1949202-OB).

2.4. Pre-Classification Image Processing

The image processing workflow (Figure 3) first included georeferencing and mosaicking together individual drone images corresponding to each multispectral band using Pix4Dmapper software v.4.6.4 (Pix4D, Prilly, Switzerland). In the processing options, the template used for mosaicking was Advanced Multispectral. Different settings were attempted to create the best mosaic, and the final processing options used were as follows. In the initial processing step, the key points image scale was set to full, defining that tie points were automatically extracted from the full size of the imagery. Tie points were features that could be detected in more than one overlapping image and formed the three-dimensional point cloud that was used to photogrammetrically orthorectify the image mosaics. Additional points were computed for every 4th pixel (densification), and every point was re-projected in a minimum of three overlapping images. Orthomosaics (photogrammetrically orthorectified image mosaics) were output in GeoTiff file format and calibrated in reflectance for each MicaSense band using images of the calibrated Spectralon panel.
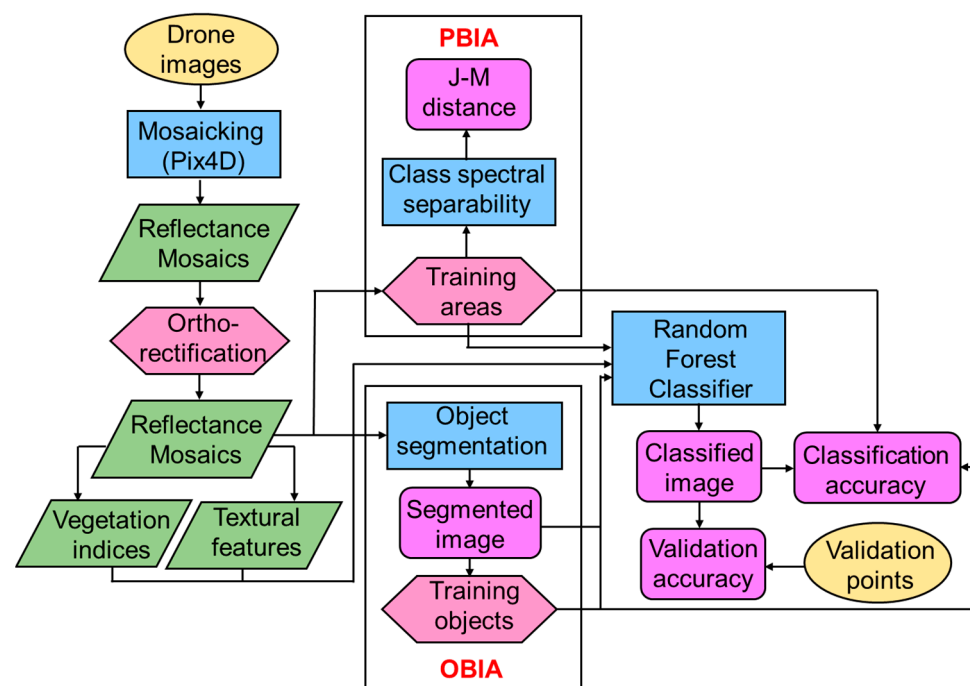
Figure 3. Flowchart of method used for processing multispectral drone images.

Among the possible processing options, many of those selected required the greatest amount of computational random-access memory (RAM), and we chose them with the goal of maximizing the quality of our calibrated reflectance mosaics. Lower-quality orthomosaics could include gaps or result in lower spatial resolutions, which we wanted to avoid as this could have reduced our ability to assess small-scale differences that are common in salt marsh vegetation communities. For future projects, constructing less dense point clouds would reduce the computational burden, but tests should be conducted to determine how this affects classification accuracy.

For our project, a 3D textured mesh was not generated because the three-dimensional aspects of the sites were not necessary to create high-quality two-dimensional maps. A 3D textured mesh represents the surface geometry of an object/scene and is created by connecting points within the 3D point cloud. Digital Surface Models (DSMs) and Digital Terrain Models (DTMs) were also not generated for our project because we did not have appropriate elevation data to evaluate their accuracy. We conducted preliminary assessments of DSM and DTM accuracies by subtracting them, creating a canopy height model (CHM), and comparing this to field measurements of plant height. Unfortunately, the CHMs included many negative values and did not correlate with plant heights, which

is why we excluded the DSMs and DTMs. Overall, among the many processing options available in Pix4D, project managers must assess their needs and computational resources when determining which to use.

To ensure that the reflectance mosaics generated from the imagery acquired each month were properly aligned, they were orthorectified using OrthoEngine in the PCI Catalyst software (PCI Geomatics Group Inc., Richmond Hill, ON, Canada). Orthorectified reflectance mosaics were clipped using the Clip function in PCI Catalyst Focus to isolate areas of interest, which were then used to compute vegetation indices and textual features using an EASI script in Catalyst. Many vegetation indices have been developed in various contexts, and the 28 vegetation indices we selected were valuable in previous studies of vegetation mapping (Table 4).

Table 4. Vegetation indices calculated from the ten-band MicaSense imagery.

Vegetation Index (VI)	Abbreviation	Formula	Reference
Normalized Difference VI	NDVI-1 NDVI-2	$(NIR842 - Red650)/(NIR842 + Red650)$ $(NIR842 - Red668)/(NIR842 + Red668)$	[63]
Normalized Difference Aquatic VI	NDAVI-1 NDAVI-2	$(NIR842 - Blue444)/(NIR842 + Blue444)$ $(NIR842 - Blue475)/(NIR842 + Blue475)$	[64]
Green Normalized Difference VI	GNDVI-1 GNDVI-2	$(NIR842 - Green531)/(NIR842 + Green531)$ $(NIR842 - Green560)/(NIR842 + Green560)$	[65]
Normalized Difference Red Edge VI	NDRE-1 NDRE-2 NDRE-3	$(NIR842 - RedEdge705)/(NIR842 + RedEdge705)$ $(NIR842 - RedEdge717)/(NIR842 + RedEdge717)$ $(NIR842 - RedEdge740)/(NIR842 + RedEdge740)$	[66]
Normalized Green VI	NG-1 NG-2	$Green531/(NIR842 + Red650 + Green531)$ $Green560/(NIR842 + Red668 + Green560)$	[67]
Difference VI	DVI-1 DVI-2	$NIR842 - Red650$ $NIR842 - Red668$	[68]
Green Difference VI	GDVI-1 GDVI-2	$NIR842 - Green531$ $NIR842 - Green560$	[69]
Normalized Red VI	NR-1 NR-2	$Red650/(NIR842 + Red650 + Green531)$ $Red668/(NIR842 + Red668 + Green560)$	[67]
Normalized Near Infrared VI	NNIR-1 NNIR-2	$NIR842/(NIR842 + Red650 + Green531)$ $NIR842/(NIR842 + Red668 + Green560)$	[67]
Green Ratio VI	GRVI-1 GRVI-2	$NIR842/Green531$ $NIR842/Green560$	[70]
Red Ratio VI	RVI-1 RVI-2	$NIR842/Red650$ $NIR842/Red668$	[71]
Red Edge Ratio VI	RERVI-1 RERVI-2 RERVI-3	$NIR842/RedEdge705$ $NIR842/RedEdge717$ $NIR842/RedEdge740$	[72]
Water Adjusted VI	WAVI-1 WAVI-2	$(1.5(NIR842 - Blue444))/((NIR842 + Blue444) + 0.5)$ $(1.5(NIR842 - Blue475))/((NIR842 + Blue475) + 0.5)$	[64]

Textural features contain information about the spatial distribution of tonal variations within an image. Textural features were calculated using the gray-level co-occurrence matrix (GLCM) method [73]. GLCM examines the spatial relationship among pixels within a defined kernel size, which was set to 9 in our study. For each of the 10 MicaSense band reflectance images, we calculated 10 textural features (Table 5), for a total of 100 per month.

OB classification was conducted using Object Analyst in PCI Catalyst and required pre-processing steps, including image segmentation and attribute calculation. Images were segmented using the 10 raw reflectance bands from each month as the source channels. The parameters used for image segmentation were as follows: scale value of 5, shape value of 0.5, and compactness value of 0.5. We tested the effect that different scale values had on classification accuracy and determined that, in general, classification accuracy decreased as the scale value increased (results not published). Following this assessment, we used the smallest scale value to ensure that image objects represented as much of the site's

heterogeneity as possible. Shape and compactness parameters ranged from 0 to 1.0, and default values in Object Analyst were used, but these parameters do not have a large effect on segmentation results for imagery of wetlands [53]. The shape parameter controls how much the segmentation is based on spectral information versus object shape information, and the compactness parameter controls how much the object shape tends to be spatially compact versus spectrally homogeneous (but less compact). After image objects were created, attributes (including raw reflectances, vegetation indices, and textural features) were calculated using average values of all pixels within each image object.

Table 5. Textural features calculated for each of the ten MicaSense bands (adapted from [73]).

Textural Feature	Formula (*)
Homogeneity	$\sum_{i=0}^{N-1}\sum_{j=0}^{N-1}\frac{P(i,j)}{1+(i-j)^2}$
Contrast	$\sum_{i=0}^{N-1}\sum_{j=0}^{N-1}P(i,j)(i-j)^2$
Dissimilarity	$\sum_{i=0}^{N-1}\sum_{j=0}^{N-1}P(i,j)\lvert i-j\rvert$
Mean	$\sum_{i=0}^{N-1}\sum_{j=0}^{N-1}iP(i,j)$
Standard deviation	$\left[\sum_{i=0}^{N-1}\sum_{j=0}^{N-1}P(i,j)(i-\mu_i)^2\right]^{1/2}$
Entropy	$\sum_{i=0}^{N-1}\sum_{j=0}^{N-1}-P(i,j)\log_e(P(i,j))$
Angular second moment	$\sum_{i=0}^{N-1}\sum_{j=0}^{N-1}P(i,j)^2$
Angular correlation	$\sum_{i=0}^{N-1}\sum_{j=0}^{N-1}\frac{P(i,j)(i-\mu_i)(j-\mu_j)}{\sigma_i*\sigma_j}$
GLDV angular second moment	$\sum_{i=0}^{N-1}v(k)^2$
GLDV entropy	$\sum_{i=0}^{N-1}(-v(k))\log_e(v(k))$

(*) N = number of grey levels, $P(i, j)$ = probability of grey tonal values i and j occurring in adjacent pixels in the original image within the window defining the neighborhood, i = digital number value of a target pixel, j = digital number value of its immediate neighbor, μ = mean tonal value, and σ = standard deviation of tonal values. $v(k)$ is a vector of the normalized gray level differences, and k = $\lvert i - j\rvert$.

2.5. Image Classification and Accuracy Assessment

Images were classified using a supervised algorithm applied to pixels or objects. The algorithm required the delineation of training areas or objects for each landcover class. We considered a total of 30 classes (Table 1), which included 6 monocultures of vegetation dominated by singular species; 3 mixed assemblages of vegetation; 6 abiotic landscape features, including rocks, driftwood, bare muddy areas, etc.; 5 classes associated with water features of the sites; and 10 classes that changed from month to month. Separate classifications were conducted for the restoration and reference sites, and some classes were observed in only one site. In total, 15 classes were used for the restoration site and 24 for the reference site, with 9 used for both sites.

For PB classification, training areas were primarily delineated as 5-pixel-by-5-pixel square polygons, although smaller and more irregularly shaped polygons were sometimes used in heterogeneous areas. Training areas were used to compute the Jeffries–Matusita (JM) distance between class pairs, which is a measure of class spectral separability. JM distances range from 0 to 2, with values of 2 representing class pairs that are completely separated [74]. JM distances were computed for each month using 10 band reflectance images. For OB classification, training objects were identified using the centroid of training polygons prepared for PB classifications. In total, the classification of the reference site used

539 training polygons and 535 validation polygons for 24 classes, and the classification of the restoration site used 440 training polygons and validation polygons for 15 classes (Figure 4). We used JM distance values from each month to assess how acquisition time affected the spectral separability of the classes used in our study, which, in turn, affected the classification accuracies.
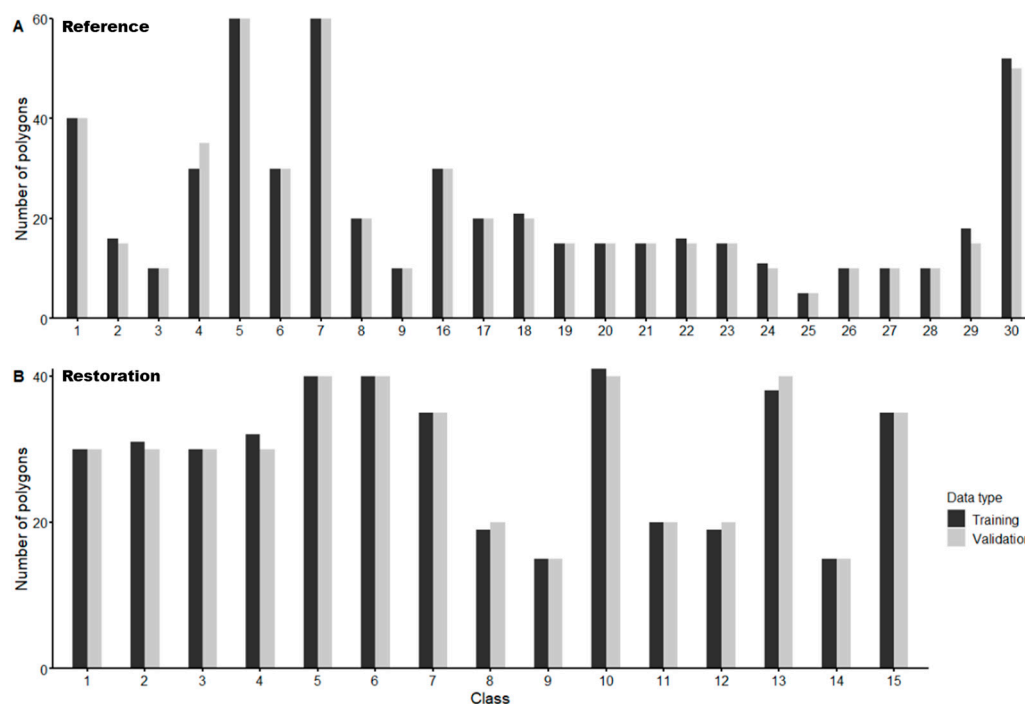
Figure 4. Number of training and validation polygons used for each landcover class used in classifications of western (**A**) reference (Site A) and (**B**) restoration (Site B) sites in Aulac. See Supplementary Figures S3 and S4 for maps showing spatial distributions of training and validation data.

The mixed-pixel problem occurs when, at the scale of observation, several classes contribute to the observed spectral response of a pixel. For our project, the scale of observation was ~7 cm, and salt marsh vegetation communities commonly have multiple species growing amongst one another within that scale, which contributes to the mixed-pixel problem. We addressed this problem by including classes of mixed vegetation in areas where multiple species grew together in an area of less than ~49 cm^2 (area of a pixel). Many of our mixed classes occurred in the reference site (Site A), as is typical in established salt marshes in the region. In the restoration site (Site B), the plant community primarily consists of monocultures which produce pure, unmixed pixels; still, mixed pixels can occur in boundary areas where one monoculture transitions to another. A limitation of our study was that we did not have landcover classes to represent every type of mixed pixel.

We used Random Forest (RF), a non-parametric decision tree-type supervised classification algorithm. RF can be executed in R (script written by Ned Horning using the packages maptools, sp, randomForest, raster, and rgal), which we used for the PB classifications. We used the "all-polygon" version of the algorithm, which considers all the pixels within training area polygons and does not use average values. For OB classification, we used the Random Trees classifier in PCI Catalyst Object Analyst, which uses the same method as the RF algorithm we used for PB classifications. We applied PB and OB classifications to raw reflectances, vegetation indices, and textural features extracted from the multi-temporal drone imagery acquired in June, July, and August over the reference and restoration sites.

RF classification algorithms randomly sampled all pixels or objects as candidates at each node in the forest, which included 500 independent decision trees with the default mtry

variable. The value of the default mtry variable is the square root of p, where p is the number of variables in x (i.e., the matrix of predictors for the classification). Within each decision tree, two-thirds of the training data were randomly selected ("in-bag" data; IB) to develop it. This tree was validated using the remaining third of the data ("out-of-bag" data; OOB). This process was repeated for 500 decision trees and produced 500 independent classifications which, once combined, produced the final classification map. Finally, RF ranked the degree of importance of each image variable (consisting of reflectances of individual MicaSense bands, vegetation indices, and textural features) in the classification [75]. Rankings were based on the mean decrease in accuracy of each input variable. Mean decrease in accuracy expresses how much OOB accuracy (described below) the model loses by excluding a variable; the more the accuracy suffers, the more important the variable.

Classification accuracy was assessed in two ways. First, OOB training data were compared to classified images. This was carried out using a confusion matrix, where each cell expressed the number of pixels in each class defined by OOB data with the number classified to it. The confusion matrix allowed for computing average and overall accuracies, kappa coefficients, as well as individual user's and producer's accuracies (UAs and PAs) for each class. The second accuracy assessment was conducted by comparing the classified image to validation field data. For each validation data point, classes were extracted from the classified image using the Extract Values to Points tool of ArcMap®. Confusion matrices and associated accuracies were then computed.

3. Results

3.1. Class Spectral Separability

Reflectance values of landcover classes' training areas (used for PB classification) were well separated from one another, as indicated by a mean JM distance ranging from 1.94 to 1.97 (Table 6). Because separability values were calculated using data from singular months, we could use these results to assess temporal variability in the landcover class spectral signatures and determine the best month for differentiating certain class pairs. For the reference site, July imagery achieved the lowest average JM distance. For the restoration site, class pairs achieved, on average, higher JM distance values when using July and August imagery compared to using June imagery. Despite adequate average JM distance values, many pairs had low values (<1.90), indicating that they were not well separated. While low JM distances must be considered, our classifications were completed using additional input features of vegetation indices and textures that have improved classification accuracies in the past [36,76] but were not included in the JM distance calculations. In addition, many of our classes represented areas that changed from month to month, and it was expected that these classes would have low separability values when analyzed one month at a time. This is why we used multi-temporal images for producing the final map and why we did not include low JM distance values generated using the change classes during our interpretation of separability results.

Landcover class pairs with low inter-class separability values largely included the vegetation classes (Table 6). These class pairs were expected to achieve the lowest JM distance values because the variation in reflectance between types of vegetation is much smaller than it is between more spectrally contrasting class pairs (e.g., vegetation classes when paired with deep water). In the reference site, the classes most prevalently included in pairs with low separability were mixed vegetation ones (Classes 17 and 30). In addition, low separability values were generated between *Triglochin* (Class 16) and *S. alterniflora* classes, likely resulting from their having similar morphologies and because they often both grew in mixed assemblages with *S. patens*. For imagery of the restoration site, class pairs with low separability values in each month were *S. alterniflora* (clean, dense) and *S. alterniflora* (clean, sparse) (Classes 6 and 13); *S. pectinata* and dike vegetation (Classes 12 and 15); and rocks and compacted soil (light) (Classes 3 and 10). We found that differences in *S. alterniflora* density did not affect reflectance characteristics to a degree that resulted in good separability. Also, the reflectance characteristics of *S. pectinata* and other vegetation

growing in high-elevation areas lining the perimeter of the site were not distinct enough to produce high JM distance values. Despite having relatively low separability in all three months, *S. alterniflora* (clean, dense) and *S. alterniflora* (clean, sparse) class pairs were most spectrally distinct in August, while *S. pectinata* and dike vegetation were least spectrally distinct in August.

Table 6. JM distances computed using reflectance values of PB training areas extracted from original reflectance images for 10 MicaSense bands acquired for Aulac reference (Site A) and restoration (Site B) sites in June, July, and August 2021. Landcover class pairs < 1.90 for each set of images listed in ascending order. Class pairs, including change classes, omitted from this table. See Supplementary Tables S2 and S3 for values of all class pairs.

Site	Month	Average JM Distance Value	Minimum JM Distance Value	Class Pairs with JM Distance Values < 1.90
Reference (Site A)	June	1.96	1.21	7 and 17 (mixed mid-elevation vegetation), 16 (*Triglochin*) and 30 (mixed *S. alterniflora* and *S. patens*), 17 and 30, 6 and 7, 6 and 17, 5 and 16, 7 and 30, 6 and 30, 5 and 30
	July	1.95	1.07	7 and 17, 6 and 7, 16 and 30, 17 and 30, 5 and 30, 7 and 30, 18 (floating green algae) and 21 (submerged aquatic vegetation), 6 and 17, 6 and 30, 5 and 16, 16 and 17
	August	1.96	1.21	7 and 17, 16 and 30, 17 and 30, 6 and 7, 5 and 17, 5 and 16, 7 and 30, 6 and 30, 5 and 30
Restoration (Site B)	June	1.94	1.15	6 (*S. alterniflora* clean, dense) and 13 (*S. alterniflora* clean, sparse), 5 (*S. alterniflora* muddy) and 13, 5 and 6, 12 (*S. pectinata*) and 15 (dike vegetation), 3 (rocks) and 10 (compacted soil light), 2 (compacted soil dark) and 3, 6 and 7 (*S. patens*), 7 and 13
	July	1.97	1.58	7 and 12, 5 and 6, 12 and 15, 3 and 10, 6 and 13
	August	1.97	1.72	12 and 15, 3 and 10, 7 and 12, 7 and 15, 6 and 13, 2 and 3

3.2. Classification

Overall OOB accuracies were >99% when using multi-temporal image sets for both PB and OB methods (Tables 7 and 8). It is common for RF classifiers to achieve very high out-of-bag accuracy when working with many input variables [33,36,40], and many studies that use RF choose to not present OOB accuracy assessments. We have presented these values because they display how effective the RF classifiers were at assigning training area pixels to the correct classes, and it is valuable to understand how high these values can be when using hundreds of input variables, as we did (we used 414). PB multi-temporal classifications of the reference and restoration sites achieved 0.1–0.2% higher OOB classification accuracy than OB classification did. High individual OOB UA and PA were achieved during both classifications for both methods. The relatively low UAs and PAs achieved during PB and OB classification of the reference site were a result of confusion between *S. alterniflora* (muddy) (Class 5) and mixed *S. alterniflora* and *S. patens* (Class 30) during OB classification, but no confusion occurred during PB classification. For the restoration site, OOB classification error was primarily the result of confusion between *S. pectinata* (Class 12) and dike vegetation (Class 15). PB classification also showed confusion between classes 1 and 2, 3 and 10, and 4 and 11. It should be remembered that more data were used in the calculation of PB OOB accuracies, because the classifier considered all pixels within training areas rather than singular objects (i.e., groups of pixels), and so one misclassification during OB classification resulted in a greater loss of accuracy than a few misclassifications during PB classification.

Table 7. The reference site (Site A) out-of-bag classification accuracies (in %) computed by PB and OB Random Forest classifiers when applied to the 2021 multi-temporal image sets. See Supplementary Table S4 for full confusion matrices.

Class Number	Class Name	OOB Accuracy			
		PB		OB	
		UA	PA	UA	PA
1	Bare mud exposed to air	100	100	100	100
2	Compacted soil (dark)	100	100	100	100
3	Rocks/eroded shoreline pieces	100	100	100	100
4	Wrack	100	100	100	100
5	*Spartina alterniflora* (muddy)	100	100	100	98.3
6	*Spartina alterniflora* (clean, dense)	100	100	100	100
7	*Spartina patens*	100	100	100	100
8	Deep salt pool water	100	100	100	100
9	Bare mud exposed to air → clean, dense *S. alterniflora*	100	100	100	100
16	*Triglochin maritima*	100	100	100	100
17	Mixed mid-elevation vegetation (*S. patens*, *Puccinellia*, etc.)	100	100	100	100
18	Floating green algae (Chlorophyta)	100	100	100	100
19	Emerged salt pool mud → shallow salt pool water	100	100	100	100
20	Emerged salt pool mud (salty)	100	100	100	100
21	Submerged aquatic vegetation	100	100	100	100
22	Deep salt pool water → floating green algae	100	100	100	100
23	Deep salt pool water (June) → submerged aquatic vegetation (July, August)	100	100	100	100
24	Deep salt pool water (June, July) → submerged aquatic vegetation (August)	100	100	100	100
25	Shallow salt pool water	100	100	100	100
26	Shallow salt pool water → submerged aquatic vegetation	100	100	100	100
27	Floating green algae → submerged aquatic vegetation → shallow salt pool water	100	100	100	100
28	Floating green algae → deep salt pool water	100	100	100	100
29	Wrack → vegetated areas of *S. alterniflora* and *S. patens*	100	100	100	100
30	Mixed vegetation: *S. alterniflora* and *S. patens*	100	100	98.1	100
	Average accuracy	100		99.8	
	Overall accuracy	100		99.8	
	Kappa coefficient	100		99.8	

Table 8. The restoration site (Site B) out-of-bag classification accuracies (in %) computed by PB and OB Random Forest classifiers when applied to the 2021 multi-temporal image sets. See Supplementary Table S5 for full confusion matrices.

Class Number	Class Name	OOB Accuracy			
		PB		OB	
		UA	PA	UA	PA
1	Bare mud exposed to air	99.9	100	100	100
2	Compacted soil (dark)	100	99.9	100	100
3	Rocks/eroded shoreline pieces	99.7	100	100	100
4	Wrack	100	99.9	100	100
5	*Spartina alterniflora* (muddy)	100	100	100	100
6	*Spartina alterniflora* (clean, dense)	100	100	100	100
7	*Spartina patens*	100	100	100	100
8	Deep salt pool water	100	100	100	100
9	Bare mud → *S. alterniflora* (clean, dense)	100	100	100	100
10	Compacted soil (light)	100	99.8	100	100
11	Wood	99.6	100	100	100
12	*Spartina pectinata*	99.6	100	100	95.0
13	*S. alterniflora* (clean, sparse)	100	100	100	100
14	*S. alterniflora* → wrack	100	100	100	100
15	Dike vegetation	100	99.8	97.2	100
	Average accuracy	99.9		99.7	
	Overall accuracy	99.9		99.8	
	Kappa coefficient	99.9		99.8	

The resulting classified maps produced by PB and OB classifications of multi-temporal images showed the distribution of classes in the sites (Figure 5 for the reference site (A) and Figure 6 for the restoration site (B)).

3.3. Variable Importance

The RF classifier provided a ranking of input variables based on their relative mean decrease in accuracy when omitted. We used 414 total input variables, with 138 generated per image acquisition. For multi-temporal PB classification of the reference site, 8 (32%), 6 (24%), and 11 (44%) of the top 25 input variables were from imagery acquired in June, July, and August, respectively, with 3 (12%), 9 (36%), and 13 (52%) for the OB classifications (Tables 9 and 10). For the restoration site, 4 (16%), 10 (40%), and 11 (44%) of the top 25 input variables were from imagery acquired in June, July, and August, respectively, for the PB classifications, with 5 (20%), 4 (16%), and 16 (64%) for the OB classifications. For each classification, input variables from August were most prevalent in the top 25. The input variables from July greatly outnumbered the ones from June during the PB classification of the restoration site and the OB classification of the reference site but were slightly outnumbered by those from June during the PB classification of the reference site and OB classification of the restoration site. Overall, the imagery acquired in August consistently provided more than a third of the top 25 ranked variables in the classifications.

Figure 5. Classified images of the western reference site in Aulac (Site A) created using (**A**) pixel- and (**B**) object-based (right) Random Forest classifiers applied to 414 input features from imagery acquired on 13 June, 12 July, and 10 August 2021 to map (**C**) 24 classes.
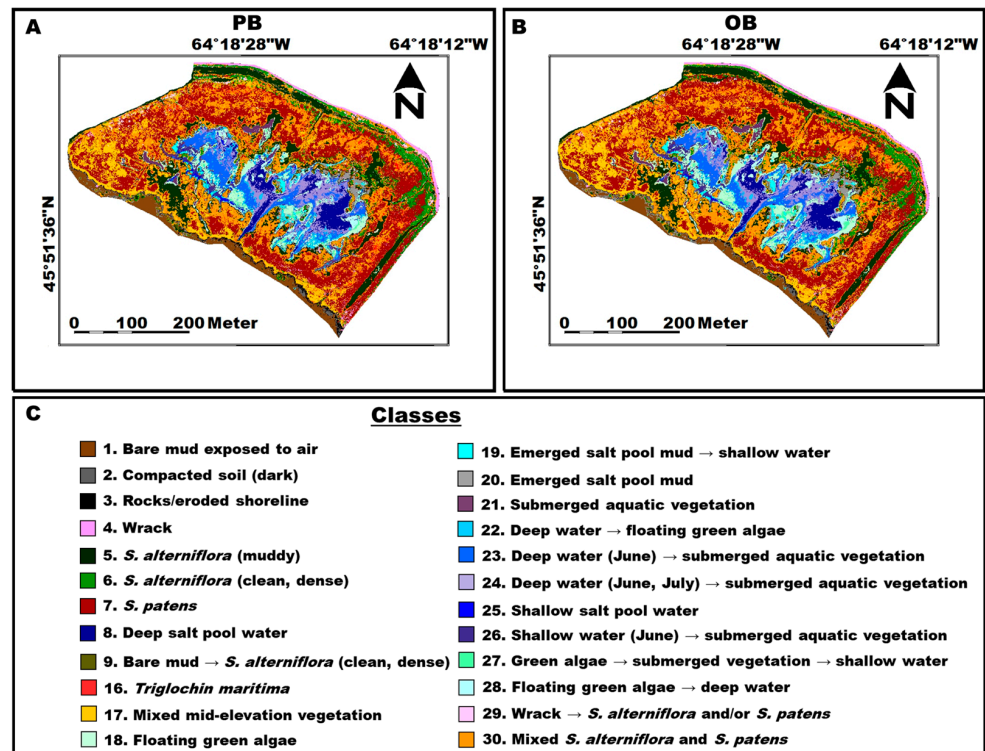

Figure 6. Classified images of the western restoration site in Aulac (Site B) created using (**A**) pixel- and (**B**) object-based Random Forest classifiers applied to 414 input features from imagery acquired on 13 June, 12 July, and 10 August 2021 to map (**C**) 15 classes.
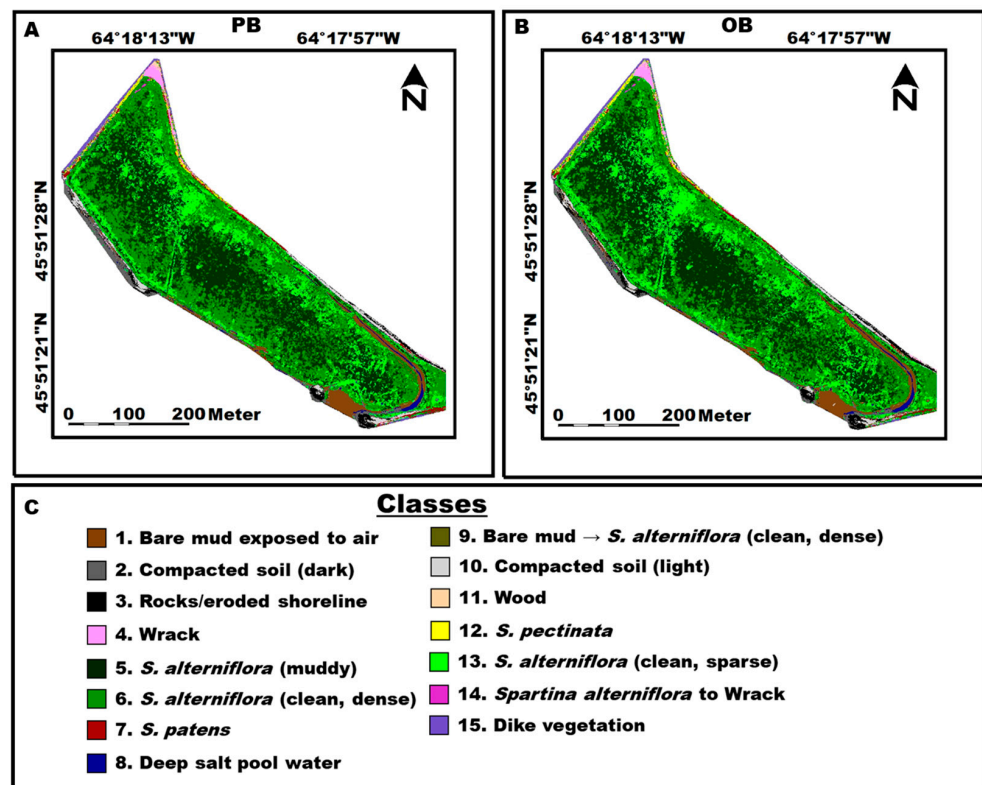
Table 9. Top 25 input variables of the reference site (Site A) ranked according to the mean decrease in accuracy computed by PB and OB Random Forest classifications applied to the 2021 multi-temporal images. See Supplementary Table S6 for full rankings.

Rank	PB	OB
1	RedEdge717_TextureMean_August	RedEdge740_TextureMean_July
2	Green560_TextureMean_July	Red668_August
3	Red668_TextureMean_August	Red668_TextureMean_August
4	RedEdge705_TextureMean_August	Green531_August
5	Green560_TextureMean_August	NIR842_July
6	Green560_TextureAngCorrelation_August	NNIR-1_July
7	Green531_TextureMean_August	Red650_TextureMean_August
8	Green531_TextureAngCorrelation_August	RedEdge705_TextureMean_August
9	Red650_TextureMean_August	RedEdge717_TextureMean_August
10	RedEdge717_August	Green560_August
11	NDVI.2_June	RedeEdge717_August
12	RedEdge717_TextureAngCorrelation_June	NIR842_TextureMean_July
13	NR.2_June	Green560_TextureMean_August
14	RedEdge705_August	GNDVI-2_July
15	Green531_July	NG-2_July
16	Blue444_TextureMean_June	RedEdge705_August
17	NDAVI.1_June	RedEdge740_July
18	Red668_TextureMean_June	NDVI-2_June
19	RVI.2_June	Green531_TextureMean_August
20	Red668_August	Red668_July
21	Green531_TextureMean_July	RERVI-1_June
22	Green531_TextureAngCorrelation_July	NG-1_July
23	RedEdge740_TextureMean_July	Red650_August
24	Blue475_TextureMean_June	Blue475_August
25	RedEdge717_TextureAngCorrelation_July	NR-2_June

Among the 138 total input variables extracted from each month's imagery, 10 (7%) were raw reflectance bands, 28 (20%) were vegetation indices, and 100 (73%) were textural features. For each site, the same 414 input variables were used for both classification approaches. The most important raw reflectance bands for both approaches were the Green, RedEdge, and Red bands. The Blue band was also ranked high for the OB classification of the reference site. Raw reflectance bands were overrepresented in the top 25 variables of each classification compared to their representation in the dataset. For the PB classifications, raw reflectance bands made up 4 (16%) and 3 (12%) of the top 25 variables for the reference and restoration sites, respectively, and 9 (36%) and 5 (20%) for the OB classifications. Vegetation indices that appeared in the top 25 variables of at least two of our classifications were Normalized Red (NR), Normalized Difference (NDVI), Normalized Near Infrared (NNIR), Green Ratio (GRVI), Red Ratio (RVI), and Normalized Difference Aquatic (NDAVI). The only vegetation index that was not among the top variables of any of our classifications was the Water Adjusted Vegetation Index (WAVI). Only 4 (16%) and 2 (8%) of the 25 top input variables for our PB classifications of the reference and restoration sites, respectively, were vegetation indices. Conversely, vegetation indices comprised 8 (32%) and 15 (56%) of the top 25 ranking variables for the OB classifications. The tonal mean calculation was the

most common highly ranked measure of texture during all our classifications, and textures calculated using the reflectance bands Red, Green, Blue, RedEdge, and NIR were all among the top 25 most important variables. For the PB classifications, 17 (68%) and 20 (80%) of the top 25 input variables for the classification of images over the reference and restoration sites, respectively, were textural features (Tables 9 and 10). OB classifications had fewer textural features in the top 25 variables (8 and 5, for the reference and restoration sites, respectively), but the tonal mean calculation was again the most important.

Table 10. Top 25 input variables of the restoration site (Site B) ranked according to the mean decrease in accuracy computed by PB and OB Random Forest classifications applied to the 2021 multi-temporal images. See Supplementary Table S7 for full rankings.

Rank	PB	OB
1	RedEdge740_TextureAngCorrelation_August	NR-2_August
2	Green531_TextureMean_July	Blue475_August
3	Green531_July	NDAVI-1_August
4	Green560TextureMean_August	NR-1_August
5	NIR842_TextureMean_June	NIR842_TextureMean_June
6	GRVI.2_June	Red668_August
7	Red668_TextureMean_July	GNDVI-2_July
8	RedEdge717_TextureMean_August	RedeEdge717_August
9	NIR842_TextureMean_August	NNIR-1_June
10	Blue444_TextureMean_August	Green560_TextureMean_August
11	Red650_TextureMean_June	NDRE-1_July
12	Blue444_TextureMean_July	GNDVI-1_August
13	RedEdge740_TextureMean_August	Blue475_TextureMean_August
14	NIR842_TextureMean_July	Green560_August
15	Green560_July	DVI-2_June
16	Red650_TextureMean_July	NDVI-1_August
17	NNIR.1_June	NNIR-2_August
18	Green531_TextureMean_August	Red650_August
19	Green531_TextureContrast_August	Green560_TextureMean_June
20	RedEdge717_August	Green531_TextureMean_August
21	Blue444_TextureAngCorrelation_August	GNDVI-2_August
22	RedEdge717_TextureSt.Dev_August	GRVI-1_July
23	Blue475_TextureMean_July	GDVI-1_August
24	Blue444_TextureAngCorrelation_July	RVI-1_June
25	RedEdge717_TextureDissimilarity_July	NDAVI-2_July

3.4. Validation Accuracy

Validation accuracy is a more reliable measure of classification accuracy than OOB accuracy because it compares the classified image with an independent set of validation data (Tables 11 and 12). For the reference site, classification using multi-temporal imagery achieved overall validation accuracies of 92.4% and 91.1% for PB and OB classifications, respectively. The vegetation community was dominated by *S. patens*, which was often found growing in mixed assemblages with other salt marsh species, including *S. alterniflora*, *Triglochin*, *Puccinellia*, *Lysimachia*, *Plantago*, *Solidago*, *Argentina*, and *Limonium*. The *S. patens* class covered more area than any other and had reductions in accuracy due to confusion

with *S. alterniflora* (clean, dense) (Class 6), mixed mid-elevation vegetation (Class 17), mixed *S. alterniflora* and *S. patens* (Class 30), and the change class bare mud to *S. alterniflora* (Class 9). *Spartina alterniflora* covered less area in the reference site than in the restoration site. *Spartina alterniflora* (dense, muddy) (Class 5) had a UA and PA >93.0% for both classification methods, but confusions with *Triglochin* (Class 16) and mixed *S. alterniflora* and *S. patens* (Class 30) were responsible for classification errors. *Spartina. alterniflora* (clean, dense) (Class 6) was mapped with more error than the previous class because of confusion with two mixed vegetation classes (Classes 17 and 30). *Triglochin* (Class 16) was mapped with greater error of commission during PB classification but greater error of omission during OB classification. Mixed vegetation classes were often misclassified as one another and as the other vegetation types. Multi-temporal RF classifiers performed well at identifying landcover classes that changed in the reference site. The average UA and PA of the change classes (Classes 9, 19, 22, 23, 24, 26, 27, 28, and 29) were 97.4% and 95.6%, respectively, for PB classification and 96.5% and 94.3% for OB classification. Most of these classes were associated with the large salt pool (depression that holds water at low tide) in the site.

Table 11. Reference site (Site A) validation class accuracies (in %) computed by PB and OB Random Forest classifiers when applied to 2021 multi-temporal image sets. See Supplementary Table S4 for full confusion matrices.

		OOB Accuracy			
		PB		OB	
Class Number	Class Name	UA	PA	UA	PA
1	Bare mud exposed to air	86.7	97.5	88.1	92.5
2	Compacted soil (dark)	100	86.7	100	80.0
3	Rocks/eroded shoreline pieces	80.0	80.0	75.0	90.0
4	Wrack	100	96.7	96.7	96.7
5	*Spartina alterniflora* (muddy)	98.2	93.3	96.6	95.0
6	*Spartina alterniflora* (clean, dense)	87.5	93.3	80.0	93.3
7	*Spartina patens*	93.2	91.7	94.6	88.3
8	Deep salt pool water	100	100	100	100
9	Bare mud exposed to air → clean, dense *S. alterniflora*	100	100	100	90.0
16	*Triglochin maritima*	75.7	93.3	83.9	86.7
17	Mixed mid-elevation vegetation (*S. patens*, *Puccinellia*, etc.)	96.2	83.3	92.3	80.0
18	Floating green algae (Chlorophyta)	95.0	95.0	95.0	95.0
19	Emerged salt pool mud → shallow salt pool water	100	93.3	100	93.3
20	Emerged salt pool mud (salty)	100	86.7	85.7	80.0
21	Submerged aquatic vegetation	93.3	93.3	92.9	86.7
22	Deep salt pool water → floating green algae	92.9	86.7	93.3	93.3
23	Deep salt pool water (June) → submerged aquatic vegetation (July, August)	100	100	93.8	100
24	Deep salt pool water (June, July) → submerged aquatic vegetation (August)	100	100	90.9	100
25	Shallow salt pool water	100	100	100	100
26	Shallow salt pool water → submerged aquatic vegetation	100	90.0	100	90.0
27	Floating green algae → submerged aquatic vegetation → shallow salt pool water	100	90.0	100	90.0
28	Floating green algae → deep salt pool water	90.0	100	90.9	100
29	Wrack → vegetated areas of *S. alterniflora* and *S. patens*	93.8	100	100	93.3
30	Mixed vegetation: *S. alterniflora* and *S. patens*	89.4	84.0	83.0	88.0
	Average accuracy	93.9		92.4	
	Overall accuracy	92.4		91.1	
	Kappa coefficient	91.9		90.5	

Table 12. Restoration site (Site B) validation class accuracies (in %) computed by PB and OB Random Forest classifiers when applied to 2021 multi-temporal image sets. See Supplementary Table S5 for full confusion matrices.

Class Number	Class Name	Validation Accuracy			
		PB		OB	
		UA	PA	UA	PA
1	Bare mud exposed to air	100	100	96.8	100
2	Compacted soil (dark)	100	96.7	100	86.7
3	Rocks/eroded shoreline pieces	100	100	100	100
4	Wrack	96.6	93.3	96.6	93.3
5	*Spartina alterniflora* (muddy)	100	100	90.9	100
6	*Spartina alterniflora* (clean, dense)	100	95.0	86.8	82.5
7	*Spartina patens*	97.0	91.4	93.9	88.6
8	Deep salt pool water	100	100	100	100
9	Bare mud → *S. alterniflora* (clean, dense)	100	86.7	92.9	86.7
10	Compacted soil (light)	92.7	95.0	97.4	95.0
11	Wood	95.2	100	100	100
12	*Spartina pectinata*	93.8	75.0	94.1	80.0
13	*S. alterniflora* (clean, sparse)	93.0	100	90.5	95.0
14	*S. alterniflora* → wrack	100	100	93.8	100
15	Dike vegetation	84.2	94.1	86.5	91.4
	Average accuracy	95.5		94.0	
	Overall accuracy	95.2		93.2	
	Kappa coefficient	94.8		92.6	

For the restoration site, multi-temporal image classification achieved overall validation accuracies of 95.5% and 94.0% for PB and OB classifications, respectively. Most of the restoration site was covered by a monoculture of *S. alterniflora* with varying appearance based on its density, the soil moisture content, and the amount of mud on plant leaves (Classes 5, 6, and 13). When using the multi-temporal image set, the average UA and PA of these classes were 95.2% and 98.3%, respectively, for PB classification and 89.4% and 92.5% for OB classification. For PB classification, lower validation accuracies were a result of confusion between *S. alterniflora* (clean, dense) (Class 6), *S. patens* (Class 7), and dike vegetation (Class 15) and between *S. alterniflora* (clean, sparse) (Class 13), *S. patens* (Class 7), and change class bare mud to *S. alterniflora* (Class 9). For OB classification, lower validation accuracies resulted from confusion between the classes mentioned above and with one another. *Spartina patens* was mapped with a UA and PA of 97.0% and 91.4%, respectively, for PB classification and 93.9% and 88.6% for OB classification. Reductions in the validation accuracy for this class (*S. patens*) were due to confusion with Class 6 (*S. alterniflora* (clean, dense)), Class 13 (*S. alterniflora* (clean, sparse)), and Class 15 (dike vegetation). *Spartina pectinata* (Class 12) has been important during restoration dynamics in our sites, but at the time of image acquisition, it was only found growing in a low density along the high-elevation dike areas and showed some confusion with the dike vegetation class (Class 15). Both PB and OB classifiers were able to accurately identify change classes, although there was some confusion in OB classification between the *S. alterniflora* to wrack (Class 14) and wrack classes (Class 4) and in both classifications between bare mud to *S. alterniflora* (Class 9) and *S. alterniflora* (clean, dense) (Class 6) and *S. alterniflora* (clean sparse) (Class 13) classes.

4. Discussion

Our primary goal was to determine which classification method, pixel- or object-based, was higher performing and more suitable for monitoring coastal vegetation, using an 11-year-old restoring salt marsh and an established (reference) salt marsh in the upper Bay of Fundy as a case study. A secondary goal was to evaluate the relative importance of input variables (raw reflectances, vegetation indices, and textural features) in our multi-temporal classifications and determine which month(s) of the growing season (June, July, or August) provided the most important variables. We also took the opportunity to test the effectiveness of landcover classes representing areas on the ground that changed throughout our multi-temporal image sets; such change classes may be useful to assess longer time-scale changes, including year-to-year ones, occurring during restoration. Achieving our goals will help to optimize the methodology for remote sensing recovery trajectories of salt marshes in the future. Below, we discuss how and why the PB classifier may have outperformed the OB classifier; how the RF classifier generally compares to other commonly used approaches; how the most important input variables varied among the months and classification approaches; considerations related to classifying environments with strong seasonal and annual variation; how using many landcover classes, including those that focus on change in a multi-temporal image set, affect classification results; challenges associated with remote sensing studies, including ours; and recommendations for future classifications assessing annual salt marsh recovery patterns.

4.1. Comparison of Classification Approaches

In our study, PB RF classifiers outperformed OB RF classifiers in overall validation accuracy (92.4% and 95.2% vs. 91.1% and 93.2%). With very-high-spatial-resolution imagery, it is usually recommended to use OB classification methods to reduce "salt-and-pepper" effects in classified maps that can result from PB classification [27]. A methodological contributor to our comparative result may be that the OB classification was conducted on an inadequately segmented image; a poor-quality segmentation directly leads to a low-quality classification [77]. Furthermore, we used an unsupervised segmentation method that could have incorrectly grouped pixels into too many (over-segmentation) or too few (under-segmentation) objects that did not represent single homogenous classes [49]. As has been mentioned, achieving optimal segmentation is difficult in wetlands with relatively small plants and highly spatial heterogenous vegetation communities [51]. Upon selecting the most suitable method, parameters (including shape, compactness, and size), and input variables for segmentation can be difficult to optimize because of the high spatial variation and low spectral variation in coastal wetland plant communities [53]. PB classification methods are typically more user-friendly than OB methods because they do not require selection and optimization of segmentation parameters. Further work is needed to optimize the segmentation method to improve the accuracy of OB image classification in the case of our salt marsh sites.

Despite the recent popularity of OB classification methods, which many studies have shown a preference for in mapping coastal wetlands [27,40,53], our study found that the PB RF classification approach achieved a higher validation accuracy. Among the studies directly comparing PB and OB methods and mapping coastal wetlands with drone imagery [50,52], our results aligned with those of Martinez-Prentice et al. [50], who found that PB classifiers performed better. Differing results between studies are likely influenced by the nature of the coastal wetland under investigation. The Zheng et al. [52] study, where OB methods outperformed PB methods, was conducted in a sub-tropical (31 degrees latitude) salt and brackish marsh at the mouth of an estuary along the Yellow Sea, which had plant communities consisting of *Phragmites* sp., *Scirpus triqueter*, *Carex scabrifolia*, and *Imperata cylindrica* [78] (reeds, bulrushes, and cogon grasses, respectively); these plants are larger, with more showy inflorescences, than the plants of the Aulac marshes. On the other hand, Martinez Prentice et al.'s [50] study was conducted in a north temperate coastal wetland (58 degrees latitude) along the Baltic Sea, where the plant communities

include moor grasses (*Molinia caerulea*) and rushes (*Carex panicea*) [79]. These Baltic coastal meadows include vegetation that resembles the grasses of the Aulac marshes in size and inflorescence. The physical sizes of plants in the type of coastal wetland investigated could be a large contributor to whether a PB or OB classification technique better maps vegetation patterns.

Many classification algorithms are widely available and selecting the appropriate one can be difficult. For our study, we used RF-supervised classification approaches. Random Forest, which has been used to achieve high classification accuracies for mapping salt marshes and other coastal wetlands [33,34,36,40,50,54], is considered easily accessible (including within the free software R v4.2.3) and requires relatively few pre-defined parameters. In addition, the structure of the RF classifier is more easily understood than those of deep learning classifiers, including Artificial Neural Networks, which use hidden layers. Despite this, more research investigating deep learning classifiers should be conducted because they can outperform machine learning classifiers, including RF [38,52], although another study found the opposite [54]. Deep learning networks require more intensive computational power and longer training times than RF but have the potential to achieve higher validation accuracies, even with fewer input variables [35]. Many other classification approaches have shown potential for accurate mapping of coastal wetlands [27,32,40,60], and additional approaches are continually being developed. Overall, environmental monitoring project managers need to assess their needs and resources when selecting a classification algorithm for accurate mapping, but the results of our and other studies have shown that RF is a user-friendly option that can achieve very high classification accuracies that compare with other, more complex classifiers.

4.2. Similarities and Differences in Variable Importance between Classification Approaches

In our multi-temporal RF classifications, the most highly ranked variables differed for the PB and OB classifications but were a combination of raw reflectances, vegetation indices, and textural features from each month for both classifier types. Raw reflectance bands were more prevalent among the top 25 input variables for the OB classifications than for the PB classifications; nonetheless, all our classifications had a larger representation of raw reflectance bands among the top variables above that among the total number of input variables. The first studies using remote sensing to monitor coastal wetlands typically relied on raw reflectance alone [80] and achieved accuracies ranging from ~70 to 90% [26,31,81,82]. As expected, none of the raw reflectances extracted from the June images was among the top variables in our classifications because above-ground vegetative biomass had just started to emerge and likely showed less variation in reflectance compared to when it was more developed later in the growing season. Among the raw reflectance bands in the top 25 input variables, the RedEdge bands were unsurprisingly included; they have been found useful for discriminating vegetation types [83]. In particular, the RedEge portion of a graminoid (the primary plant taxon in the Aulac marshes) canopy is largely affected by inundation [84], and so RedEdge bands may be especially useful for classifying the vegetation of intertidal salt marshes, where water levels regularly fluctuate. The other raw reflectance bands among the top 25 variables included the occasional Red, Green, and Blue (RGB) band, supporting that RGB bands can be useful for classifying wetland vegetation [52,54,83]. Previous studies have accurately mapped coastal wetlands without RedEdge and NIR bands [52], and the minimum number and required types of bands necessary to accurately map salt marsh vegetation should be further investigated. If RGB bands are capable of accurately mapping habitats without RedEdge and NIR, a project's cost could decrease, since RGB sensors are more readily available and affordable. The NIR band, which was not among the most important input variables in our classifications, has also been found to be less important for distinguishing wetland vegetation previously [54]; it is correlated with leaf thickness [85], and the graminoids dominating the Aulac marshes have very thin leaves. While there were differences in the number of important raw reflectance bands between classification approaches, this importance was more consistent between PB

and OB classifications than for the other types of input variables (vegetation indices and textural features).

A major difference in the top 25 most important input variables between our PB and OB classifications was a greater occurrence of vegetation indices in the latter classification. Vegetation indices are now almost always used in classifications of coastal wetlands [37,86] and have also been used to accurately quantify vegetation biomass and canopy moisture [42,87]. Similar to our expectations for the raw reflectance input variables, we expected the June vegetation indices to be less important than those extracted from the July and August images. Surprisingly, the vegetation indices among the most important variables were all extracted from June images in the PB classifications, although it is unclear why. In the OB classifications, however, vegetation indices extracted from the July and August images were more important than those extracted from the June ones. Our results suggest that segmenting an image into objects may increase the importance of vegetation indices and decrease the importance of textural features during the classification of salt marshes (discussed further in the next paragraph).

The sizeable difference in the importance of textural features between our PB and OB classifications suggests that texture is more important when analyzing an image using a smaller base unit of analysis (individual pixels) than it is when using a larger base unit of analysis (image objects) and supports the notion that texture is strongly influenced by spatial resolution [88]. Textural features in classification are useful in sites like salt marshes that have classes with little inter-class spectral variability and high within-class variability [27,56]. We found that the tonal mean calculation always ranked very high for our classifications, as also reported previously [83]. While textural features extracted from the imagery of each month were important, those extracted from the August images were most prevalently featured among the top 25 input variables of our classifications. This may be because August is when vegetation is fully grown and variations in its spatial characteristics are elevated [54]. While there were differences in the input variables considered important for each classification, both classifications were similar in that those from August prevailed. Overall, understanding the importance of input features relative to their acquisition times is useful information when streamlining methodologies for remotely monitoring wetlands, including those undergoing change.

4.3. Further Classification Considerations for Temporal Change, Both Seasonal and Annual

With our multi-temporal images (collected at monthly intervals during the growing season), we found that imagery acquired in August was more useful for distinguishing landcover classes than imagery acquired in June and July, and, in general, imagery acquired in July was more useful than imagery acquired in June. Previous studies have also found that variation in spectral characteristics and vegetation indices between coastal vegetation types is greatest later in the growing season when vegetation is fully grown, particularly when it is flowering [39,89], which typically occurs in August in Atlantic Canadian salt marshes [23]. Furthermore, our study and others have [29,30] determined that multi-temporal classification of coastal wetlands achieves higher validation accuracies than single-temporal classification for habitats with strong seasonality [87,90,91] like our north temperate salt marshes [23]. Note that these short-term studies used multi-temporal imagery acquired within a single year, whereas longer-term image analyses of coastal wetland change typically used images acquired at one time per year [56,92,93].

Beyond overall validation accuracy, other considerations come into play when selecting an appropriate remote sensing methodology for detecting temporal change in vegetative communities. Using multi-temporal images within a growing season may complicate the analysis of long-term annual change by introducing within-year variation and many images. The financial cost and effort required increase with the number of image acquisitions, since resources must be put towards additional ground-truthing and image processing. Therefore, the type of change that is of interest (within or between years) should be considered when determining the necessary frequency of image acquisitions

per year. For assessing restoration dynamics, annual changes are often of greater interest than within-year changes [23,60]. Note, though, that early in a restoration project, multiple (monthly) monitoring times have been central to uncovering certain fast changing dynamics [59]. Additionally, restoration occurring in sub-optimal or deteriorating conditions may need frequent monitoring for the quick implementation of adaptive management strategies [21]. Thus, the decision on whether to have (or how many) multiple image acquisition times for a given year may depend on the age and/or environmental conditions of the restoration project. Based on the results of our study, for long-term monitoring of salt marsh vegetation dynamics, we recommend acquiring one or two images annually, specifically when vegetation has fully grown and is flowering. Nevertheless, there may be situations where imagery from both early and late in a growing season is necessary. In the next section, we further discuss quantifying temporal change in salt marshes by comparing our method using change classes with other commonly used methods.

4.4. Assessment of Number of Landcover Classes, including Change Classes

The number and nature of landcover classes used during a classification greatly influence the resulting map. In our study, we used a relatively large number of salt marsh landcover classes (24 and 15) and achieved overall OOB and validation accuracies greater than 90%. Our classification of the restoration site (15 classes) achieved a higher validation accuracy than that of the reference site (24 classes). Many previous studies with similar or higher validation accuracies (88–95%) used fewer classes (five classes with 95% [56], five classes with 88% [52], and eight classes with 90% [28]). Studies experimenting with a similar number of classes (17) typically achieved lower accuracies than our study (57–86%) [31,35], and a classification that used 43 classes only achieved 58% [27]. While we did have many classes, separating the mixed vegetation classes into individual species classes could make them more spectrally homogonous and potentially increase classification accuracy. However, this could also increase the classification error due to the mixed-pixel problem, and, in general, using more classes increases the probability of misclassification. Note that in our study, mixed vegetation classes helped address the small-scale (within a 49 cm^2 area) heterogenous plant communities. We considered having more of them but lacked enough appropriate training and validation data because these mixed landcovers did not cover substantial areas within the sites. Previous studies mapping coastal wetlands have also used mixed vegetation classes to address the spatial heterogeneity of coastal wetlands and the mixed-pixel problem [35,40,46]. Other studies using very high spatial resolutions avoid the use of mixed classes [37,38,42,54] and rarely directly discuss how they address mixed pixels or their implications. As in previous studies, our classes with contrasting spectral properties, including our deep salt pool water, wood, and shallow salt pool water classes (Classes 8, 11, and 25, respectively), were more likely to be correctly identified by the classifiers (high validation PA, >95%) and be reliably mapped (high validation UA, >95%) [35,40]. On the other hand, the classes with lower UAs and/or PAs were those with spectral and textural properties that were more similar to those of other classes. Many of our change classes, including Classes 15, 19, 23, 24, 27, 28, and 29, achieved high (>90%) validation UAs and PAs because of their spectrally contrasting properties caused by their variation within the multi-temporal images. Overall, the objectives of a study, the spatial resolution of the imagery, and the prevalence of mixed pixels must be considered when determining the appropriate number and type of landcover classes for a classification. Additionally, the landcover classes should be determined at the beginning of a project, so that appropriate field validation data can be collected for each class. The number of landcover classes and the quality and quantity of field data greatly influence the result of a classification, which highlights the importance of establishing meaningful landcover classes and building strong training and validation datasets.

While we developed change classes within a single growing season (from an image set containing three acquisition times), such classes could be applied to an image set spanning multiple years. Representing change as individual classes has been used to assess temporal

patterns in Eucalyptus forests in Brazil [55] and coastal areas, including salt and brackish marshes, in Texas, USA [56], but has never been used to monitor salt marsh restoration. An advantage of using change classes in a single classification is that the importance of variables from each image in the set can be extracted, providing insight into which acquisition time was most important. However, as the number of classes in a classification increases, coinciding with the amount of change observed and the number of images in the set, more processing time is required, and results are often harder to interpret. Instead of using change classes, change assessment is most often conducted as a post-classification technique [32,55,93], where change is more easily interpreted in the form of a confusion matrix. Post-classification techniques do not require the creation of change classes but do require classifications representing before and after change, which are then compared [46]. This method could be applied to single images and used to assess sequential within- and between-year differences, rather than classifying multiple images together. We do not recommend using change classes to assess within-year differences (as we did in our study) in combination with interannual post-classification analysis because it is unlikely that the same seasonal changes would occur in the same spatial locations in multiple years, and so change would be overestimated. If using multi-temporal images within and between years, we recommend that either every image in the time series should be classified individually and change assessed with post-classification analysis (both within and between years), or that a general map excluding change classes should be created for each year and then compared using post-classification change analysis [32].

4.5. Challenges and Future Research in Remote Sensing of Salt Marshes

The process of selecting remote sensing and image analysis methods for environmental monitoring can be daunting. Each project comes with its own set of unique goals and conditions, and the learning curve for acquiring and processing images can be steep. Moreover, with the continuous development of new technology and methods, staying up to date adds to the complexity. Environmental managers need to be mindful of their project objectives, budget constraints, and knowledge limitations when choosing appropriate remote sensing methods. Consulting with remote sensing experts can simplify this process. In the initial project planning phase, understanding the required image spatial resolution and survey area size is central to determining whether satellite or drone imagery is more suitable. Subsequently, consideration must be given to the number of required images and the selection of appropriate remote sensing methods tailored to the desired project outcomes, ranging from simple visual assessments to complex classification models [46]. Some trial and error with various image processing methods may be necessary to optimize the approach for a specific environmental monitoring project. Additionally, considering local ecological knowledge of the landcovers and biotic communities at the sites is necessary to ensure that high-quality training and validation data are created and that meaningful objectives are pursued. For our study, we had this knowledge because we have been sampling the sites since 2010 (i.e., the beginning of the Aulac salt marsh restoration project) [23,59,60]. Overall, the quality of an environmental management project is enhanced through a cross-disciplinary approach, involving collaboration among experts in remote sensing, ecology, geology, sociology, and other relevant fields to broaden the collective knowledge base.

Addressing the challenges encountered in our study that may have influenced result quality is instructive. Initially, our field data acquisition was not intended to evaluate every individual landcover class. Instead, our sampling focused on assessing ecological changes in salt marsh restoration and reference sites, following the field methods outlined in Virgin et al. [60]. Consequently, we gathered numerous field data points for the most abundant vegetation landcovers but fewer points for landcovers around the site perimeters or within the large salt pool in the reference site (Site A). To overcome this challenge, we augmented training and validation data for these less sampled landcovers using our knowledge of the sites and aerial photographs, which has previously been carried out with success [40]. Additionally, the Geographic Positioning System (GPS) we utilized had a spatial accuracy

of 2–3 meters, meaning that GPS points collected during our fieldwork did not always precisely represent the sampled area. This spatial inaccuracy was a notable challenge, especially in a salt marsh, where landcover variations occur at centimeter scales. Future studies needing ground-truthing should consider employing centimeter-accuracy RTK GPS units during field data collection. Despite these challenges, we maintain confidence in the accuracy of the training and validation points, as we have expert knowledge of the field sites through extensive annual sampling and could perform appropriate corrections. A further study component that we could have conducted is testing more than one classifier (in addition to Random Forests) for our study system. We chose RF because it is known to perform well, based on our experience [36,94] and other studies in the literature [33,34,40,50,54]. However, a focused comparative analysis with other algorithms could have revealed a higher-performing option, as documented in other studies [52]. Another study component (alluded to above) is to evaluate the minimum number and required types of spectral bands needed to accurately map salt marsh vegetation. Moreover, evaluating the inclusion of additional sensors and remote sensing platforms could have enhanced the comprehensiveness and informativeness of our study to guide future remote sensing of salt marsh restoration projects (see below).

Since the integration of multispectral drone data in coastal environmental monitoring projects has become widespread, many future research efforts are needed to guide and extend their utility in coastal vegetation mapping, in addition to the ones mentioned above. These include investigation of the effect of incorporating more landcover classes, training data, and validation data to assess improvement or diminishment of mapping accuracy [38]. Moreover, the drone camera utilized in our study, the MicaSense Dual Camera System, has similar bands to Sentinel-2 [95]. This compatibility allows for the validation of Sentinel-2-based classified images using drone imagery [96]. The synergy of drone and satellite data facilitates the assessment of environmental changes at various scales and would be particularly valuable for habitats like salt marshes which exhibit heterogeneous vegetation communities while covering extensive geographic areas. Our study solely used input variables derived from the reflectance data acquired with the MicaSense dual-camera system, and future studies could benefit from incorporating DSMs, DTMs, and canopy height models derived from RTK GPS and Lidar data. These additional data sources have been valuable in various studies [35,58], especially considering the strong influence of elevation on salt marshes and its role in driving vegetation zonation in these habitats. Overall, there are many future research directions that, if followed, will further assist with the selection of appropriate remote sensing methods for mapping salt marshes.

5. Conclusions

Our comparison of classification approaches showed that pixel-based Random Forest classifiers achieved higher classification and validation accuracies than object-based Random Forest classifiers for mapping vegetation in north temperate salt marsh sites. Our results likely partially depended on the small-sized plants at the sites; OB methods may be more appropriate for wetlands with larger-sized plants. Pixel-based approaches do not require the optimization and selection of input features for image segmentation, possibly explaining its higher performance in our case study, in addition to making it more user-friendly. We found that input variables extracted from the August images were most important in the classifications, suggesting that imagery should generally be acquired at times when vegetation is developed and flowering. Additionally, our results indicated that many image input variables, including raw reflectances, vegetation indices, and textural features, are valuable for achieving high classification accuracy and that increasing the number of input variables can be achieved by using multi-temporal image sets. Also, our results showed potential for monitoring classes that change when using multi-temporal images. The lessons learned from our study provide guidance for future monitoring projects of salt marshes in Atlantic Canada and could be applied to other geographical locations with plant sizes similar to those in the Aulac marshes. Monitoring vegetation dynamics

during coastal wetland restoration is essential because of the threatened status of these ecosystems and the need to restore the important services they provide.

References

1. He, S.; Zhenguo, N.; Chen, Y.; Li, L.; Zhang, H. Global wetlands: Potential distribution, wetland loss, and status. *Sci. Total. Environ.* **2017**, *586*, 319–327. [CrossRef]
2. Davidson, N.C.; Fluet-Chouinard, E.; Finlayson, C.M. Global extent and distribution of wetlands: Trends and issues. *Mar. Freshw. Res.* **2018**, *69*, 620–627. [CrossRef]
3. Owers, C.J.; Rogers, K.; Woodroffe, C.D. Spatial variation of above-ground carbon storage in temperate coastal wetlands. *Estuar. Coast. Shelf Sci.* **2018**, *210*, 55–67. [CrossRef]
4. Gallant, K.; Withey, P.; Risk, D.; Van Kooten, G.C.; Spafford, L. Measurement and economic valuation of carbon sequestration in Nova Scotian wetlands. *Ecol. Econ.* **2020**, *171*, 106619. [CrossRef]
5. Gyssels, G.; Poesen, J.; Bochet, E.; Li, Y. Impact of plant roots on the resistance of soils to erosion by water: A review. *Prog. Phys. Geogr. Earth Environ.* **2005**, *29*, 189–217. [CrossRef]
6. Ford, H.; Garbutt, A.; Ladd, C.; Malarkey, J.; Skov, M.W. Soil stabilization linked to plant diversity and environmental context in coastal wetlands. *J. Veg. Sci.* **2016**, *27*, 259–268. [CrossRef] [PubMed]
7. Kadlec, R.H. Wastewater treatment at the Houghton Lake wetland: Hydrology and water quality. *Ecol. Eng.* **2009**, *35*, 1287–1311. [CrossRef]
8. Straub, J.N.; Gates, R.J.; Schultheis, R.D.; Yerkes, T.; Coluccy, J.M.; Stafford, J.D. Wetland food resources for spring-migrating ducks in the Upper Mississippi River and Great Lakes Region. *J. Wildl. Manag.* **2012**, *76*, 768–777. [CrossRef]
9. Rasool, S.; Rasool, T.; Gani, K.M. Unlocking the potential of wetland biomass: Treatment approaches and sustainable resource management for enhanced utilization. *Bioresour. Technol. Rep.* **2023**, *23*, 101553. [CrossRef]
10. Pedersen, E.; Weisner, S.E.B.; Johansson, M. Wetland areas' direct contributions to residents' well-being entitle them to high cultural ecosystem values. *Sci. Total Environ.* **2019**, *646*, 1315–1326. [CrossRef] [PubMed]
11. Alikhani, S.; Nummi, P.; Ojala, A. Urban wetlands: A review on ecological and cultural values. *Water* **2021**, *13*, 3301. [CrossRef]

12. Xu, X.; Chen, M.; Yang, G.; Jiang, B.; Zhang, J. Wetland ecosystem services research: A critical review. *Glob. Ecol. Conserv.* **2020**, *22*, e01027. [CrossRef]

13. Lin, W.; Xu, D.; Guo, P.; Wang, D.; Li, L.; Gao, J. Exploring variations of ecosystem service value in Hangzhou Bay Wetland, Eastern China. *Ecosyst. Serv.* **2019**, *37*, 100944. [CrossRef]

14. Balwan, W.K.; Kour, S. Wetland—An ecological boon for the environment. *East Afr. Sch. J. Agric. Life Sci.* **2021**, *4*, 38–48. [CrossRef]

15. Zhang, W.; Ge, Z.-M.; Li, S.-H.; Tan, L.-S.; Zhou, K.; Li, Y.-L.; Xie, L.-N.; Dai, Z.-J. The role of seasonal vegetation properties in determining the wave attenuation capacity of coastal marshes: Implications for building natural defenses. *Ecol. Eng.* **2022**, *175*, 106494. [CrossRef]

16. Ballut-Dajud, G.A.; Sandoval Herazo, L.C.; Fernández-Lambert, G.; Marín-Muñiz, J.L.; López Méndez, M.C.; Betanzo-Torres, E.A. Factors affecting wetland loss: A review. *Land* **2022**, *11*, 434. [CrossRef]

17. Fluet-Chouinard, E.; Stocker, B.D.; Zhang, Z.; Malhotra, A.; Melton, J.R.; Poulter, B.; Kaplan, J.O.; Goldewijk, K.K.; Siebert, S.; Minayeva, T.; et al. Extensive global wetland loss over the past three centuries. *Nature* **2023**, *614*, 281–286. [CrossRef] [PubMed]

18. Romaña, S.S.; DeAngelis, D.L.; Koh, H.L.; Sulaiman, R.B.R.; Zhai, L. Conservation and restoration of mangroves: Global status, perspectives, and prognosis. *Ocean Coast. Manag.* **2018**, *154*, 72–82. [CrossRef]

19. Erwin, K.L. Wetlands and global climate change: The role of wetland restoration in a changing world. *Wetl. Ecol. Manag.* **2009**, *17*, 71–84. [CrossRef]

20. Humpenöder, F.; Karstens, K.; Lotze-Campen, H.; Leifeld, J.; Menichetti, L.; Barthelmes, A.; Popp, A. Peatland protection and restoration are key for climate change mitigation. *Environ. Res. Lett.* **2020**, *15*, 104093. [CrossRef]

21. Waltham, N.J.; Alcott, C.; Barbeau, M.A.; Cebrian, J.; Connolly, R.M.; Deegan, L.A.; Dodds, K.; Goodridge Gaines, L.A.; Gilby, B.L.; Henderson, C.J.; et al. Tidal marsh restoration optimism in a changing climate and urbanizing seascape. *Estuaries Coasts* **2021**, *44*, 1681–1690. [CrossRef]

22. Pickett, S.T.A.; Cadenasso, M.L.; Meiners, S.J. Ever since Clements: From succession to vegetation dynamics and understanding to intervention. *Appl. Veg. Sci.* **2009**, *12*, 9–21. [CrossRef]

23. Norris, G.S.; Virgin, S.D.S.; Schneider, D.W.; McCoy, E.M.; Wilson, J.M.; Morrill, K.L.; Hayter, L.; Hicks, M.E.; Barbeau, M.A. Patch-level processes of vegetation underlying site-level restoration patterns in a megatidal salt marsh. *Front. Ecol. Evol.* **2022**, *10*, 1000075. [CrossRef]

24. Mahdavi, S.; Salehi, B.; Granger, J.; Amani, M.; Brisco, B.; Huang, W. Remote Sensing for Wetland Classification: A Comprehensive Review. *GIScience Remote Sens.* **2018**, *55*, 623–658. [CrossRef]

25. Mirmazloumi, S.M.; Moghimi, A.; Ranjgar, B.; Mohseni, F.; Ghorbanian, A.; Ahmadi, S.A.; Amani, M.; Brisco, B. Status and trends of wetland studies in Canada using remote sensing technology with a focus on wetland classification: A bibliographic analysis. *Remote Sens.* **2021**, *13*, 4025. [CrossRef]

26. Neuenschwander, A.L.; Crawford, M.M.; Provancha, M.J. Mapping of coastal wetlands via hyperspectral AVIRIS data. In Proceedings of the IGARSS '98. Sensing and Managing the Environment. 1998 IEEE International Geoscience and Remote Sensing. Symposium Proceedings. (Cat. No.98CH36174), Seattle, WA, USA, 6–10 July 1998. [CrossRef]

27. Yu, Q.; Gong, P.; Clinton, N.; Biging, G.; Kelly, M.; Schirokauer, D. Object-based detailed vegetation classification with airborne high spatial resolution remote sensing imagery. *Photogramm. Eng. Remote. Sens.* **2006**, *72*, 799–811. [CrossRef]

28. Correll, M.D.; Hantson, W.; Hodgman, T.P.; Cline, B.B.; Elphick, C.S.; Gregory Shriver, W.; Tymkiw, E.L.; Olsen, B.J. Fine-scale mapping of coastal plant communities in the Northeastern USA. *Wetlands* **2019**, *39*, 17–28. [CrossRef]

29. Sun, C.; Li, J.; Liu, Y.; Liu, Y.; Liu, R. Plant species classification in salt marshes using phenological parameters derived from Sentinel-2 pixel-differential time-series. *Remote Sens. Environ.* **2021**, *256*, 112320. [CrossRef]

30. Zhao, Y.; Feng, D.; Yu, L.; Wang, X.; Chen, Y.; Bai, Y.; Hernández, H.J.; Galleguillos, M.; Estades, C.; Biging, G.S.; et al. Detailed dynamic land cover mapping of Chile: Accuracy improvement by integrating multi-temporal data. *Remote Sens. Environ.* **2016**, *183*, 170–185. [CrossRef]

31. Ramsey, E.W.; Laine, S.C. Comparison of Landsat thematic mapper and high resolution photography to identify change in complex coastal wetlands. *J. Coast. Res.* **1997**, *13*, 281–292.

32. Camilleri, S.; De Giglio, M.; Stecchi, F.; Pérez-Hurtado, A. Land use and land cover change analysis in predominately man-made coastal wetlands: Towards a methodological framework. *Wetl. Ecol. Manag.* **2016**, *25*, 23–43. [CrossRef]

33. Wang, X.; Gao, X.; Zhang, Y.; Fei, X.; Chen, Z.; Wang, J.; Zhang, Y.; Lu, X.; Zhao, H. Land-cover classification of coastal wetlands using the RF algorithm for Worldview-2 and Landsat 8 images. *Remote Sens.* **2019**, *11*, 1927. [CrossRef]

34. Zhang, X.; Xu, J.; Chen, Y.; Xu, K.; Wang, D. Coastal wetland classification with GF-3 Polarimetric SAR imagery by using object-oriented Random Forest algorithm. *Sensors* **2021**, *21*, 3395. [CrossRef] [PubMed]

35. Gonzalez-Perez, A.; Abd-Elrahman, A.; Wilkinson, B.; Johnson, D.J.; Carthy, R.R. Deep and machine learning image classification of coastal wetlands using unpiloted aircraft system multispectral images and LiDAR datasets. *Remote Sens.* **2022**, *14*, 3937. [CrossRef]

36. Norris, G.S.; Leblon, B.; LaRocque, A.; Barbeau, M.A.; Hanson, A.R. Effect of textural features for landcover classification of UAV multispectral imagery of a salt marsh restoration site. *Int. Arch. Photogramm. Remote Sens. Spat. Inf. Sci.* **2022**, *XLIII-B3-2022*, 951–958. [CrossRef]

37. Abeysinghe, T.; Simic Milas, A.; Arend, K.; Hohman, B.; Reil, P.; Gregory, A.; Vázquez-Ortega, A. Mapping invasive *Phragmites australis* in the Old Woman Creek Estuary using UAV remote sensing and machine learning classifiers. *Remote Sens.* **2019**, *11*, 1380. [CrossRef]

38. Huang, Y.; Lu, C.; Jia, M.; Wang, Z.; Su, Y.; Su, Y. Plant species classification of coastal wetlands based on UAV images and object-oriented deep learning. *Biodiv. Sci.* **2023**, *31*, 22411. [CrossRef]

39. Nardin, W.; Taddia, Y.; Quitadamo, M.; Vona, I.; Corbau, C.; Franchi, G.; Staver, L.W.; Pellegrinelli, A. Seasonality and characterization mapping of restored tidal marsh by NDVI imageries coupling UAVs and multispectral camera. *Remote Sens.* **2021**, *13*, 4207. [CrossRef]

40. Durgan, S.D.; Zhang, C.; Duecaster, A.; Fourney, F.; Su, H. Unmanned aircraft system photogrammetry for mapping diverse vegetation species in a heterogeneous coastal wetland. *Wetlands* **2020**, *40*, 2621–2633. [CrossRef]

41. Doughty, C.; Cavanaugh, K. Mapping coastal wetland biomass from high resolution Unmanned Aerial Vehicle (UAV) imagery. *Remote Sens.* **2019**, *11*, 540. [CrossRef]

42. Janousek, C.N.; Thorne, K.M.; Takekawa, J.Y. Vertical zonation and niche breadth of tidal marsh plants along the Northeast Pacific Coast. *Estuar. Coast.* **2019**, *42*, 85–98. [CrossRef]

43. Gallant, A. The challenges of remote monitoring of wetlands. *Remote Sens.* **2015**, *7*, 10938–10950. [CrossRef]

44. Pande-Chhetri, R.; Abd-Elrahman, A.; Liu, T.; Morton, J.; Wilhelm, V.L. Object-based classification of wetland vegetation using very high-resolution unmanned air system imagery. *Eur. J. Remote Sens.* **2017**, *50*, 564–576. [CrossRef]

45. Rebelo, L.-M.; Finlayson, C.M.; Nagabhatla, N. Remote sensing and GIS for wetland inventory, mapping and change analysis. *J. Environ. Manag.* **2009**, *90*, 2144–2153. [CrossRef]

46. Lu, D.; Mausel, P.; Brondízio, E.; Moran, E. Change detection techniques. *Int. J. Remote Sens.* **2004**, *25*, 2365–2401. [CrossRef]

47. Hussain, M.; Chen, D.; Cheng, A.; Wei, H.; Stanley, D. Change detection from remotely sensed images: From pixel-based to object-based approaches. *ISPRS J. Photogramm.* **2013**, *80*, 91–106. [CrossRef]

48. Blaschke, T. Object based image analysis for remote sensing. *ISPRS J. Photogramm.* **2010**, *65*, 2–16. [CrossRef]

49. Kotaridis, I.; Lazaridou, M. Remote sensing image segmentation advances: A meta-analysis. *ISPRS J. Photogramm.* **2021**, *173*, 309–322. [CrossRef]

50. Martínez Prentice, R.; Villoslada Peciña, M.; Ward, R.D.; Bergamo, T.F.; Joyce, C.B.; Sepp, K. Machine learning classification and accuracy assessment from high-resolution images of coastal wetlands. *Remote Sens.* **2021**, *13*, 3669. [CrossRef]

51. Windle, A.E.; Staver, L.W.; Elmore, A.J.; Scherer, S.; Keller, S.; Malmgren, B.; Silsbe, G.M. Multi-temporal high-resolution marsh vegetation mapping using unoccupied aircraft system remote sensing and machine learning. *Front. Remote Sens.* **2023**, *4*, 1140999. [CrossRef]

52. Zheng, J.-Y.; Hao, Y.-Y.; Wang, Y.-C.; Zhou, S.-Q.; Wu, W.-B.; Yuan, Q.; Gao, Y.; Guo, H.-Q.; Cai, X.-X.; Zhao, B. Coastal wetland vegetation classification using pixel-based, object-based and deep learning methods based on RGB-UAV. *Land* **2022**, *11*, 2039. [CrossRef]

53. Moffett, K.B.; Gorelick, S.M. Distinguishing wetland vegetation and channel features with object-based image segmentation. *Int. J. Remote Sens.* **2013**, *34*, 1332–1354. [CrossRef]

54. Du, B.; Mao, D.; Wang, Z.; Qiu, Z.; Yan, H.; Feng, K.; Zhang, Z. Mapping wetland plant communities using unmanned aerial vehicle hyperspectral imagery by comparing object/pixel-based classifications combining multiple machine-learning algorithms. *IEEE J. Sel. Top. Appl. Earth Obs. Remote Sens.* **2021**, *14*, 8249–8258. [CrossRef]

55. Soares, V.P.; Hoffer, R.M. Eucalyptus forest change classification using multi-date Landsat TM data. In *Multispectral and Microwave Sensing of Forestry, Hydrology, and Natural Resources*; SPIE: Bellingham, WA, USA, 1995; Volume 2314, pp. 281–291. [CrossRef]

56. Weismiller, R.A.; Kristof, S.J.; Scholz, D.K.; Auta, P.E.; Momin, S.A. Change detection in coastal zone environments. *Photogram. Eng. Remote Sens.* **1977**, *43*, 1533–1539.

57. Desplanque, C.; Mossman, D.J. Tides and their seminal impact on the geology, geography, history, and socio-economics of the Bay of Fundy, Eastern Canada. *Atl. Geol.* **2004**, *40*, 1–130. [CrossRef]

58. Millard, K.; Redden, A.M.; Webster, T.; Stewart, H. Use of GIS and high resolution LiDAR in salt marsh restoration site suitability assessments in the Upper Bay of Fundy, Canada. *Wetlands Ecol. Manag.* **2013**, *21*, 243–262. [CrossRef]

59. Boone, L.K.; Ollerhead, J.; Barbeau, M.A.; Beck, A.D.; Sanderson, B.G.; McLellan, N.R. Returning the tide to dikelands in a macrotidal and ice-influenced environment: Challenges and lessons learned. In *Coastal Wetlands: Alteration and Remediation*; Finkl, C.W., Makowski, C., Eds.; Coastal Research Library; Springer International Publishing: Cham, Switzerland, 2017; Volume 21, pp. 705–749, ISBN 978-3-319-56178-3.

60. Virgin, S.D.S.; Beck, A.D.; Boone, L.K.; Dykstra, A.K.; Ollerhead, J.; Barbeau, M.A.; McLellan, N.R. A managed realignment in the Upper Bay of Fundy: Community dynamics during salt marsh restoration over 8 Years in a megatidal, ice-influenced environment. *Ecol. Eng.* **2020**, *149*, 105713. [CrossRef]

61. Peterson, P.M.; Romaschenko, K.; Arrieta, Y.H.; Saarela, J.M. A Molecular phylogeny and new subgeneric classification of *Sporobolus* (Poaceae: Chloridoideae: Sporobolinae). *Taxon* **2014**, *63*, 1212–1243. [CrossRef]

62. Bortolus, A.; Adam, P.; Adams, J.B.; Ainouche, M.L.; Ayres, D.; Bertness, M.D.; Bouma, T.J.; Bruno, J.F.; Caçador, I.; Carlton, J.T.; et al. Supporting *Spartina*: Interdisciplinary perspective shows *Spartina* as a distinct solid genus. *Ecology* **2019**, *100*, e02863. [CrossRef] [PubMed]

63. Rouse, J.W.; Haas, R.H.; Scell, J.A.; Deering, D.W.; Harlan, J.C. *Monitoring the Vernal Advancements and Retro Gradation (Green Wave Effect) of Natural Vegetation*; NASA/GSFC Type III; NASA: Greenbelt, MD, USA, 1974; 371p.

64. Villa, P.; Mousivand, A.; Bresciani, M. Aquatic vegetation indices assessment through radiative transfer modeling and linear mixture simulation. *Int. J. Appl. Earth Obs.* **2014**, *30*, 113–127. [CrossRef]

65. Gitelson, A.A.; Jaufman, Y.J.; Merzlyak, M.N. Use of a green channel in remote sensing of global vegetation from EOS-MODIS. *Remote Sens. Environ.* **1996**, *58*, 457–459. [CrossRef]

66. Gitelson, A.A.; Merzlyak, M.N. Spectral reflectance changes associated with autumn senescence of *Aesculus hippocastanum* I. and *Acer platanoides* I. leaves: Spectral features and relation to chlorophyll estimation. *J. Plant Phys.* **1994**, *143*, 286–292. [CrossRef]

67. Sripada, R.P.; Heiniger, R.W.; White, J.G.; Meijer, A.D. Aerial color infrared photography for determining early in-season nitrogen requirements in corn. *Agron. J.* **2006**, *98*, 968–977. [CrossRef]

68. Richardson, A.J.; Wiegand, C.L. Distinguishing vegetation from soil background information. *Photogramm. Eng. Remote Sens.* **1977**, *43*, 1541–1552.

69. Sripada, R.P.; Heiniger, R.W.; White, J.G.; Weisz, R. Aerial color infrared photography for determining late-season nitrogen requirements in corn. *Agron. J.* **2005**, *97*, 1443–1451. [CrossRef]

70. Kimura, R.; Okada, S.; Miura, H.; Kamichika, M. Relationships among the leaf area index, moisture availability, and spectral reflectance in an upland rice field. *Agric. Water Manag.* **2004**, *69*, 83–100. [CrossRef]

71. Jordan, C.F. Derivation of leaf-area index from quality of light on the forest floor. *Ecology* **1969**, *50*, 663–666. [CrossRef]

72. Datt, B. Visible/near infrared reflectance and chlorophyll content in Eucalyptus leaves. *Int. J. Remote Sens.* **1999**, *20*, 2741–2759. [CrossRef]

73. Haralick, R.M.; Shanmugam, K.; Dinstein, I. Textural features for image classification. *IEEE Trans. Syst. Man Cybern.* **1973**, *SMC-3*, 610–621. [CrossRef]

74. Richards, J.A.; Jia, X. *Remote Sensing Digital Image Analysis: An Introduction*, 4th ed.; Springer: Berlin/Heidelberg, Germany, 2006; ISBN 978-3-540-25128-6.

75. Louppe, G.; Wehenkel, L.; Sutera, A.; Geurts, P. Understanding variable importances in forests of randomized trees. In Proceedings of the Advances in Neural Information Processing Systems, Lake Tahoe, NV, USA, 5–8 December 2013.

76. Fletcher, R. Using vegetation indices as input into Random Forest for soybean and weed classification. *Am. J. Plant Sci.* **2016**, *07*, 2186–2198. [CrossRef]

77. Mesner, N.; Oštir, K. Investigating the impact of spatial and spectral resolution of satellite images on segmentation quality. *J. Appl. Remote Sens.* **2014**, *8*, 083696. [CrossRef]

78. Tian, B.; Zhou, Y.; Zhang, Z.; Yuan, L. Analyzing the habitat suitability for migratory birds at the Chongming Dongtan Nature Reserve in Shanghai, China. *Estuar. Coast. Shelf Sci.* **2008**, *80*, 296–302. [CrossRef]

79. Kose, M.; Heinsoo, K.; Kaljund, K.; Tali, K. 20 years of Baltic Boreal coastal meadow restoration: Has it been long enough? *Ecology* **2020**, *29*, e13266. [CrossRef]

80. Hardisky, M.A.; Gross, M.F.; Klemas, V. Remote sensing of coastal wetlands. *BioScience* **1986**, *36*, 453–460. [CrossRef]

81. Klemas, V. Remote sensing of coastal wetland vegetation and estuarine water properties. In *Estuarine Processes*; Elsevier: Amsterdam, The Netherlands, 1977; pp. 381–403. ISBN 978-0-12-751802-2.

82. Sader, S.A.; Ahl, D.; Liou, W.S. Accuracy of Landsat-TM and GIS rule-based methods for forest wetland classification in Maine. *Remote Sens. Environ.* **1995**, *53*, 133–144. [CrossRef]

83. Li, C.; Zhou, L.; Xu, W. Estimating aboveground biomass using Sentinel-2 MSI data and ensemble algorithms for grassland in the Shengjin Lake Wetland, China. *Remote Sens.* **2021**, *13*, 1595. [CrossRef]

84. Turpie, K.R. Explaining the spectral red-edge features of inundated marsh vegetation. *J. Coast. Res.* **2013**, *29*, 1111–1117. [CrossRef]

85. Streher, A.S.; Torres, R.d.S.; Morellato, L.P.C.; Silva, T.S.F. Accuracy and limitations for spectroscopic prediction of leaf traits in seasonally dry tropical environments. *Remote Sens. Environ.* **2020**, *244*, 111828. [CrossRef]

86. Vuolo, F.; Neuwirth, M.; Immitzer, M.; Atzberger, C.; Ng, W.T. How much does multi-temporal Sentinel-2 data improve crop type classification? *Int. J. Appl. Earth Obs.* **2018**, *72*, 122–130. [CrossRef]

87. Klemas, V. Remote sensing of coastal wetland biomass: An overview. *J. Coast. Res.* **2013**, *290*, 1016–1028. [CrossRef]

88. Liu, L.; Chen, J.; Zhao, G.; Fieguth, P.; Chen, X.; Pietikainen, M. Texture classification in extreme scale variations using GANet. *IEEE Trans. Image Process* **2018**, *28*, 3910–3922. [CrossRef] [PubMed]

89. Gao, Z.G.; Zhang, L.Q. Multi-seasonal spectral characteristics analysis of coastal salt marsh vegetation in Shanghai, China. *Estuar. Coast. Shelf Sci.* **2006**, *69*, 217–224. [CrossRef]

90. Li, N.; Lu, D.; Wu, M.; Zhang, Y.; Lu, L. Coastal wetland classification with multiseasonal high-spatial resolution satellite imagery. *Int. J. Remote Sens.* **2018**, *39*, 8963–8983. [CrossRef]

91. Hentis, L.; Jurgens, C.; Mucsi, L. Seasonal multitemporal land-cover classification and change detection analysis of Bochum, Germany, using multitemporal Landsat TM data. *Int. J. Remote Sens.* **2015**, *37*, 3439–3454. [CrossRef]

92. Berberoğlu, S.; Akin, A.; Atkinson, P.M.; Curran, P.J. Utilizing image texture to detect land-cover change in Mediterranean Coastal Wetlands. *Int. J. Remote Sens.* **2010**, *31*, 2793–2815. [CrossRef]

93. Kesikoglu, M.H.; Atasever, U.H.; Dadaser-Celik, F.; Ozkan, C. Performance of ANN, SVM, and MLH techniques for land use/cover change detection at Sultan Marshes wetland, Turkey. *Water Sci. Technol.* **2019**, *80*, 466–477. [CrossRef] [PubMed]

94. Jahncke, R.; Leblon, B.; Bush, P.; Armand LaRocque, A. Mapping wetlands in Nova Scotia with multi-beam RADARSAT-2 Polarimetric SAR, optical satellite imagery, and Lidar data. *Int. J Appl. Earth Obs.* **2018**, *68*, 139–156. [CrossRef]
95. Jiang, J.; Johansen, K.; Tu, Y.-H.; McCabe, M.F. Multi-sensor and multi-platform consistency and interoperability between UAV, Planet CubeSat, Sentinel-2, and Landsat reflectance data. *GIScience Remote Sens.* **2022**, *59*, 936–958. [CrossRef]
96. Thomson, E.R.; Spiegel, M.P.; Althuizen, I.H.J.; Bass, P.; Chen, S.; Chmurzynski, A.; Halbritter, A.H.; Henn, J.J.; Jónsdóttir, I.S.; Klanderud, K.; et al. Multiscale mapping of plant functional groups and plant traits in the high arctic using field spectroscopy, UAV imagery and Sentinel-2A data. *Environ. Res. Lett.* **2021**, *16*, 055006. [CrossRef]